

*Handwritten scribbles*

23

N64 12161

MTP-P&VE-S-63-4  
October 17, 1963

OTS

CODE-X

**GEORGE C. MARSHALL**

**SPACE  
FLIGHT  
CENTER**

NASA  
603 1103

**HUNTSVILLE, ALABAMA**

TMX-9-1983

† AN INVESTIGATION OF VARIOUS PARAMETERS AFFECTING THE  
STRUCTURAL WEIGHT OF ROCKET VEHICLE NOSE CONES

By

Clyde D. Nevins  
and  
Benny W. Helton

OTS PRICE ✓

XEROX

\$

*Handwritten price*

MICROFILM

\$

*Handwritten price*



**SCIENCE AND SPACE ADMINISTRATION**

REPRODUCED BY  
NATIONAL TECHNICAL  
INFORMATION SERVICE  
U.S. DEPARTMENT OF COMMERCE  
SPRINGFIELD, VA. 22161



GEORGE C. MARSHALL SPACE FLIGHT CENTER

MTP-P&VE-S-63-4

AN INVESTIGATION OF VARIOUS PARAMETERS AFFECTING THE  
STRUCTURAL WEIGHT OF ROCKET VEHICLE NOSE CONES

By

Clyde D. Nevins  
and  
Benny W. Helton

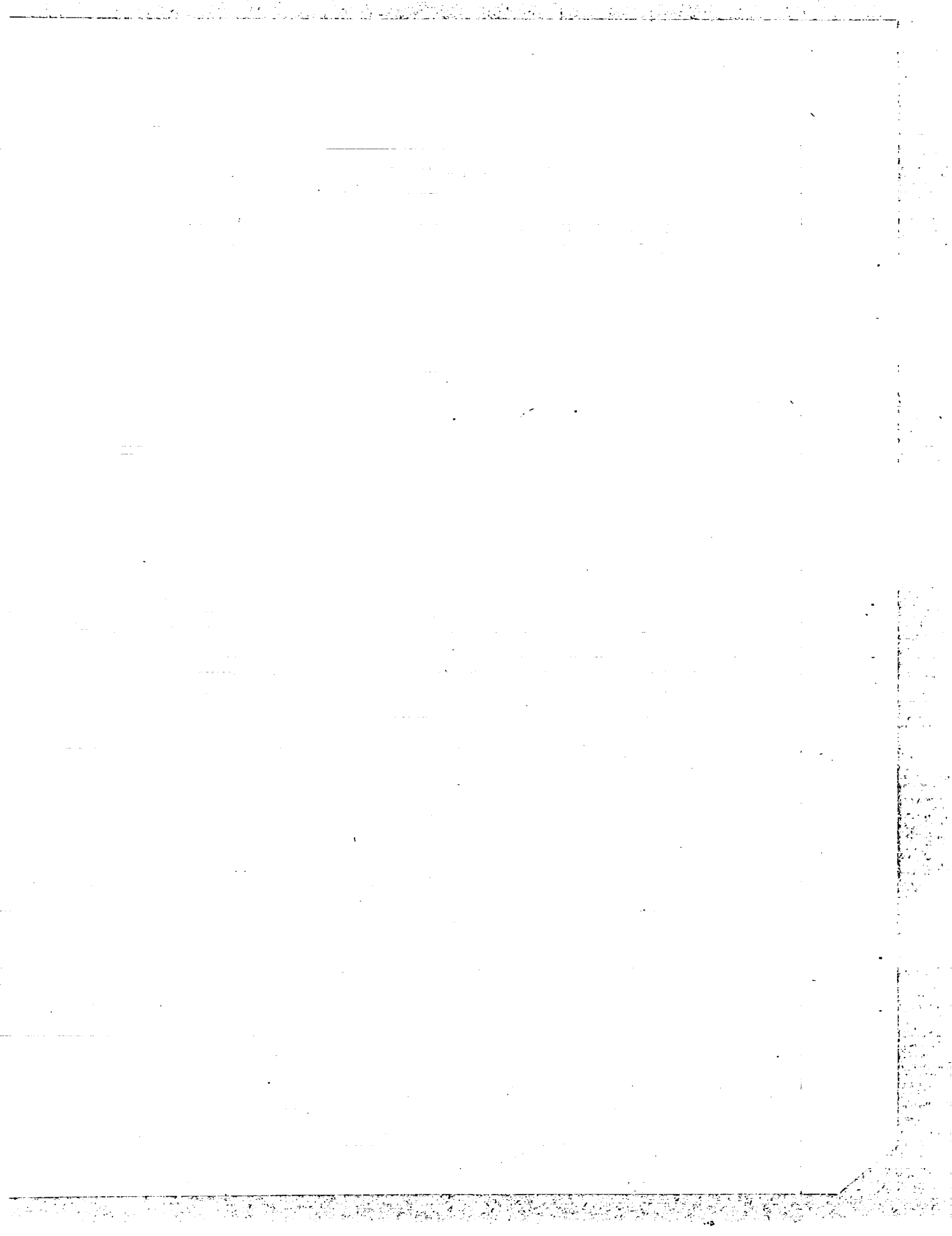
ABSTRACT

12/6/77

A series of externally pressure loaded, semi-monocoque cones, with various diameters and cone angles, were proportioned for minimum weight. The investigation was conducted to determine the cone half angle which yielded the minimum weight for a given base diameter and trajectory. In addition, the effects of alternate construction materials and blunting was investigated.

An electronic computer program was devised to make the weight optimization study. The computer results show that the cone angle producing the least weight is independent of the cone base diameter, aluminum alloy cones are lighter than fiberglass, and blunting is advantageous. A configuration other than a simple cone is recommended for study.

AUTHOR



**GEORGE C. MARSHALL SPACE FLIGHT CENTER**

---

**MTP-P&VE-S-63-4**

---

**AN INVESTIGATION OF VARIOUS PARAMETERS AFFECTING THE  
STRUCTURAL WEIGHT OF ROCKET VEHICLE NOSE CONES**

**By**

**Clyde D. Nevins**

**and**

**Benny W. Helton**

**ADVANCED STRUCTURAL DEVELOPMENT SECTION  
STRUCTURES DIVISION  
PROPULSION AND VEHICLE ENGINEERING LABORATORY**

### ACKNOWLEDGEMENT

The writers are indebted to Messers. E. L. Linsley and D. L. Bacchus of M-AERO-AA for their contribution of Appendix B and for their overall assistance in aerodynamic loading characteristics. The assistance of the Stress Section (M-P&VE-SS), particularly Mr. J. N. Nunnery, is recognized and appreciated.

Sincere appreciation is extended to Mr. J. F. Blumrich (M-P&VE-SA) for his guidance and timely suggestions throughout the course of this study and report preparation.

## TABLE OF CONTENTS

	Page
SUMMARY .....	1
INTRODUCTION .....	2
DESCRIPTION .....	3
A. Sharp Cone Analysis .....	4
B. Blunted Cone Analysis .....	10
C. Results .....	12
D. Interpretation of Results .....	26
CONCLUSIONS .....	28
APPENDIX A .....	29
APPENDIX B .....	33
REFERENCES .....	38

## LIST OF ILLUSTRATIONS

Figure	Title	Page
1.	General Cone Geometry and Configuration Schematic . . . . .	3
2.	Typical Pressure Variation for Equation 1, with Angle of Attack, $\alpha$ . . . . .	5
3.	Section through Conical Shell Frustum . . . . .	6
4.	Typical Ring Stiffener Cross Sections . . . . .	8
5.	Blunted Cone Schematic and Pressure Variation on Hemispherical Shell . . . . .	11
6.	Schematic of Typical Final Design. . . . .	13
7.	Total Cone Weight Versus Cone Half Angle; Aluminum, D = 120" . . . . .	15
8.	Total Cone Weight Versus Cone Half Angle Aluminum, D = 154" . . . . .	16
9.	Total Cone Weight Versus Cone Half Angle; Aluminum, D = 220" . . . . .	17
10.	Total Cone Weight Versus Cone Half Angle; Aluminum, D = 260" . . . . .	18
11.	Total Cone Weight Versus Cone Half Angle; Aluminum, Uniform Skin Thickness, D = 260" . . . . .	19
12.	Total Cone Weight Versus Cone Half Angle; Fiberglass, D = 260" . . . . .	20
13.	Total Weight Versus Cone Half Angle; Construction Comparison, Aluminum, D = 260" . . . . .	24
14.	Total Cone Weight Versus Cone Half Angle; Aluminum- Fiberglass Comparison, D = 260" . . . . .	25



LIST OF ILLUSTRATIONS (CONTINUED)

Figure	Title	Page
15.	Total Cone Weight Versus Cone Half Angle; Aluminum, $q$ Comparison, $D = 220''$ . . . . .	26
16.	Weight per Unit Volume Versus Cone Half Angle, Aluminum, $q = 5.6$ psi . . . . .	27
17.	Percentage Total Cone Weight Versus $d/D$ Ratio; Bluntness Effect on Total Weight. . . . .	28
18.	Normal Force Loading Schematic . . . . .	31
19.	Drag of Cones and Blunted Bodies . . . . .	34
20.	Loads on Nose Shapes $M_\infty = 1.5$ . . . . .	35
21.	Loads on Nose Shapes $M_\infty = 1.5$ . . . . .	36
22.	Cone Load Characteristics $M_\infty = 1.5$ . . . . .	37

TABLE

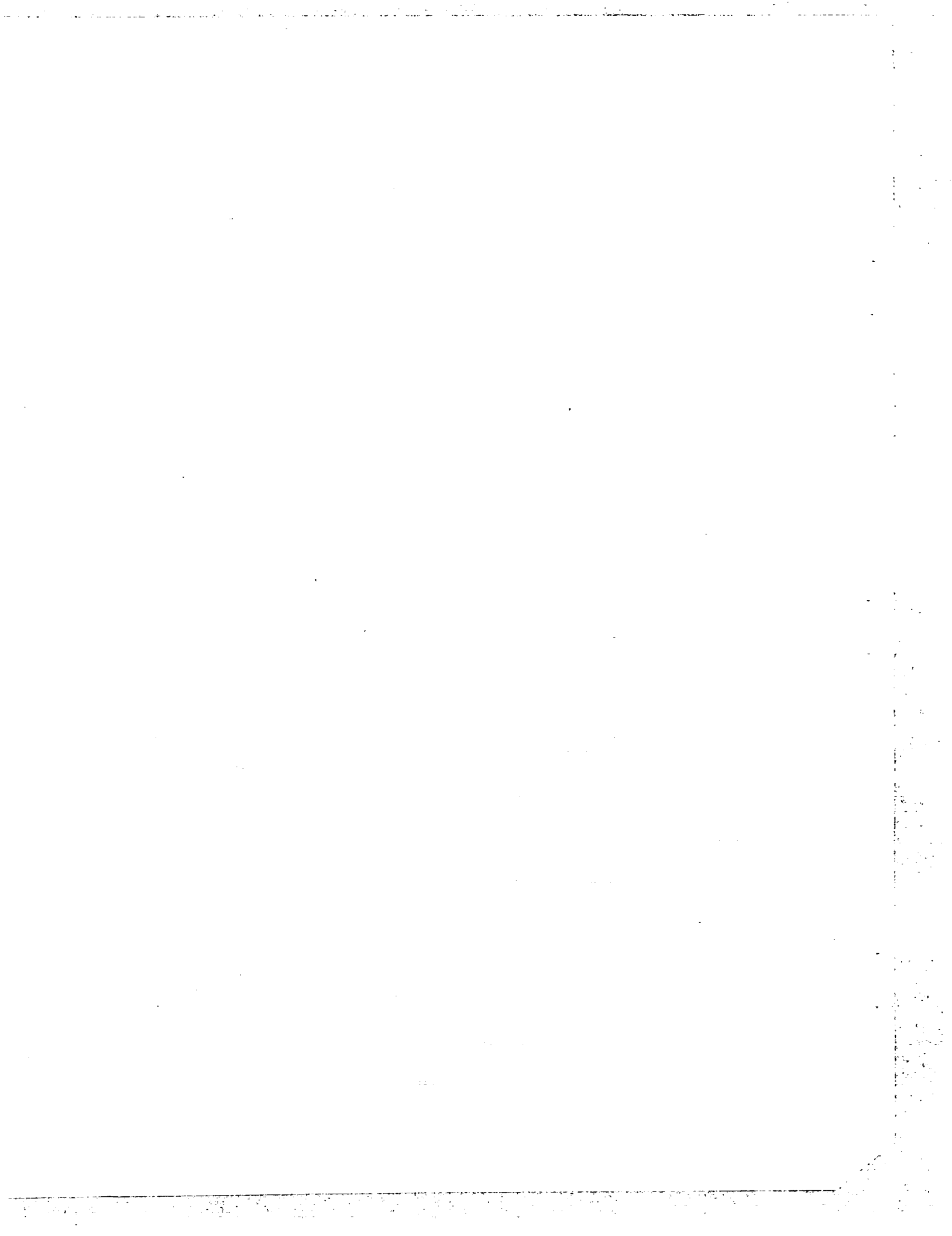
Table	Title	Page
1.	Structural Tabulations for Figure 6 . . . . .	14

## DEFINITION OF SYMBOLS

SYMBOL	DEFINITION
$a_n$	minimum diameter of cone frustum
$a_{n-1}$	maximum diameter of cone frustum
$A_R$	ring cross-sectional area
C	blunted cone pressure coefficient
D	cone base diameter
d	twice the radius of nose cap for blunted cones
$\frac{dC_x}{d(x/D)}$	axial force distribution coefficient
$\frac{dC_{z\alpha}}{d(x/D)}$	normal force distribution coefficient
E	elastic modulus
h	skin half thickness = $t/2$
$I_{req}$	required ring moment of inertia
K	hemispherical pressure constant
$K_1 =$	$\frac{4.85 \left(2 - \sqrt{\tau}\right) \left(\tau^{1-\sqrt{\tau}} - 1\right)^{1/4} \left(1 - \tau^{-1-\sqrt{\tau}}\right)^{3/4}}{\sqrt{1+\sqrt{\tau}} \left(1 - \sqrt{\tau}^2\right) \left(\tau^{2-\sqrt{\tau}} - 1\right) \ln \tau}$
$l$	length of cone frustum
L/D	caliber distance from cone apex
$N_A$	axial load per unit of circumference
$N_B$	normal load per unit of circumference

## DEFINITION OF SYMBOLS (Cont'd)

SYMBOL	DEFINITION
$N_\theta$	hemispherical shell hoop stress
$N_\varphi$	hemispherical shell meridional stress
$P_{CR}$	critical buckling pressure
$P_O$	net pressure distribution
$q$	dynamic pressure (free stream)
$r$	nose cap radius
$t$	skin thickness
$\alpha$	angle of attack in radians
$\eta$	factor of safety
$\gamma$	cone half angle
$\bar{\theta}$	$K_3 \tan \gamma \sqrt{\frac{h \cos \gamma}{a_n}}$
$\lambda$	$\frac{K_2 N_B}{P_O a_n}$
$\bar{\lambda}$	$\sqrt[4]{\frac{3(1-\nu^2)}{\sqrt{a_n(t)}}$
$\nu$	Poisson's ratio
$\sigma_{CA}$	axial membrane stress
$\sigma_{CH}$	hoop membrane stress
$\sigma_{CR}$	critical stress
$\varphi$	circumferential angle
$\varphi_2$	hemispherical shell angle
$\tau$	frustum radii ratio



GEORGE C. MARSHALL SPACE FLIGHT CENTER

---

MTP-P&VE-S-63-4

---

AN INVESTIGATION OF VARIOUS PARAMETERS AFFECTING THE  
STRUCTURAL WEIGHT OF ROCKET VEHICLE NOSE CONES

By

Clyde D. Nevins  
and  
Benny W. Helton

SUMMARY

A series of ring-stiffened, monocoque cones with base diameters of from 120 to 260 inches and with cone half angles varying from 10° to 30° were proportioned for minimum weight. Each cone was subjected to an external pressure distribution typical of that experienced during the atmospheric portion of a booster trajectory. Generally, the purpose of the investigation was to determine the optimum weight for cones within the above ranges, the optimum cone angle for specified base diameters, the weight differential between aluminum alloy and fiberglass cones, and the effects of applying various bluntness ratios to a typical cone.

A computer program was developed to make the numerous, complicated calculations in the trial and error weight optimization procedure. Short conical frustums, whose proportions were determined by local geometry and pressure conditions, were optimized with respect to weight, then were combined to form a full nose cone which was considered optimum.

Disregarding the effects of aerodynamic heating and buffeting, the results show that:

- a. A 25° half angle cone produces the least weight cone for diameters studied,
- b. Use of aluminum alloy rather than fiberglass reduces the cone weight, and
- c. Blunting the cone yields the least overall weight.

A nose fairing of alternate configuration that will utilize the results of the investigation, yet respect the downstream buffeting influence, is proposed for further study.

## INTRODUCTION

The trade-offs among structural weight, aerodynamic drag, and aerodynamic heating for nose cones of various geometries are not well established. Nose cone designs of present-day rocket vehicles, therefore, have generally assumed a cone half angle of  $15^\circ$ , a compromise with acceptable aerodynamic buffeting characteristics and short cone length. To better define the relationship between the structural weight and geometry of nose cones subjected to aerodynamic loading, a weight optimization study encompassing variations of cone angle, base diameter, and bluntness ratio was undertaken.

Monocoque cones with ring stiffeners were the only type analyzed during the course of this study, although other methods of construction were investigated for possible inclusion in the program. The use of longitudinal stringers does not efficiently aid the stability of a conical shell subjected to an external pressure. Rather, respacing of the stiffening rings has been shown to yield optimum weights for cones subjected to this loading (see Reference 1). Sandwich construction does appear to offer potential weight saving for this application. A thorough literature search, however, yielded no adequate method for optimizing a sandwich cone subjected to an external pressure. Approximate analysis methods, such as an equivalent-stiffness thickness substituted into isotropic shell equations, were shown to be highly inaccurate compared to actual test results for cylinders under external pressure (Reference 2). The accepted procedure for analysis of cylindrical sandwich shells (Reference 3) is not amenable to design since any change in structural configuration requires a solution to a sixth order determinant. The development of solutions for sandwich conical shells and the resultant complex computer program were deemed beyond the scope of this report.

The bulk of the work was done for a narrow band of maximum dynamic pressure and maximum angle of attack. An excursion into the effects of varying dynamic pressure while holding the maximum angle of attack constant was made, however, to indicate sensitivity of weight to this parameter.

In the determination of structural requirements, the internal shroud pressure has been assumed to be ambient. However, the resultant internal pressure could be above or below ambient due to the venting procedures. Further study will be made of the structural effects of an internal pressure lag.

Aerodynamic heating considerations were not incorporated into the data presented. Although the thicknesses obtained are adequate for the entire aerodynamic portion of the trajectory used, the forward-most structure may reach melting temperatures later in the trajectory if not suitably protected.

### DESCRIPTION

A conical shell is assumed to comprise the nose fairing of a rocket vehicle. Utilizing a ring-stiffened, monocoque structure, the effects of variation in geometric parameters, primarily base diameter and cone angle, on the total cone weight were investigated. Ring spacing and, in most cases, skin thickness were allowed to vary until an optimum (least weight) combination was found. External aerodynamic pressure as derived from aeroballistic data presented in Appendix B, was the only loading considered on the cone, i. e., the inertia of the cone weight, itself, was assumed negligible and any enclosed payload was assumed supported at the base diameter. The general geometry and nomenclature used in the report are presented in Figure 1.

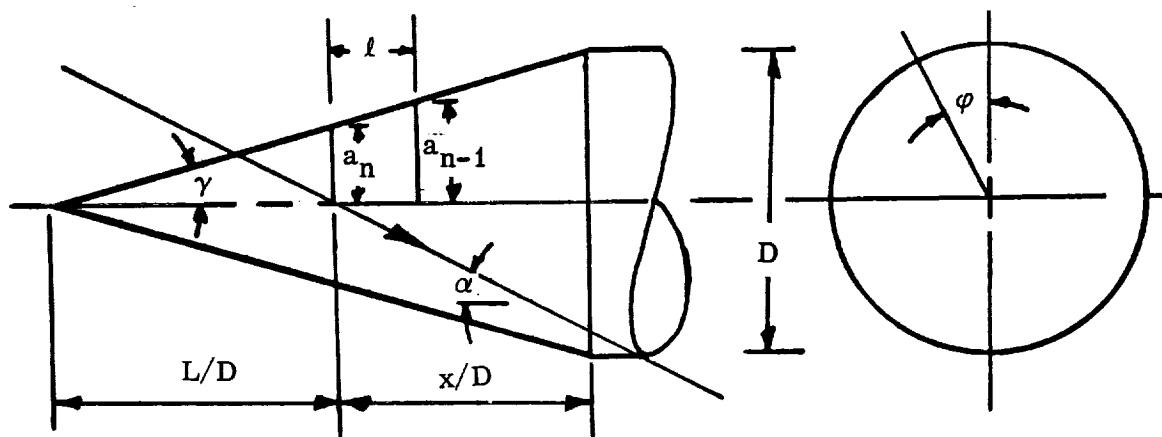


FIGURE 1. GENERAL CONE GEOMETRY AND CONFIGURATION SCHEMATIC

### A. SHARP CONE ANALYSIS

Two cases of aerodynamic loading were considered: (1) zero angle of attack ( $\alpha = 0^\circ$ ), and (2)  $7^\circ$  angle of attack, both at maximum dynamic pressure for the chosen trajectory. Case (2) provided the design condition, that being the greatest compressive force in the hoop, or circumferential, direction. Case (2) also provided the condition of maximum axial compressive force, which, incidentally, was  $180^\circ$  opposite to the maximum hoop compressive force, but this was not a critical design condition. Case (1) was checked to obtain the condition of maximum interaction between axial compression and hoop compression but this condition also proved not critical. Thus, with the aid of Figure 1, and with a given angle of attack,  $\alpha$ , the pressure distribution,  $P_o$ , around the circumference of a conical cross section for Case (2) loads is expressed by Equation 1 (See Appendix A).

$$P_o = \eta q \left\{ \frac{1}{4} \left[ \frac{dC_x}{d(x/D)} \right]_o \cot \gamma + \frac{\alpha}{2} \left[ \frac{dC_{z\alpha}}{d(x/D)} \right]_o \cos (180^\circ - \varphi) \right\}, \quad (1)$$

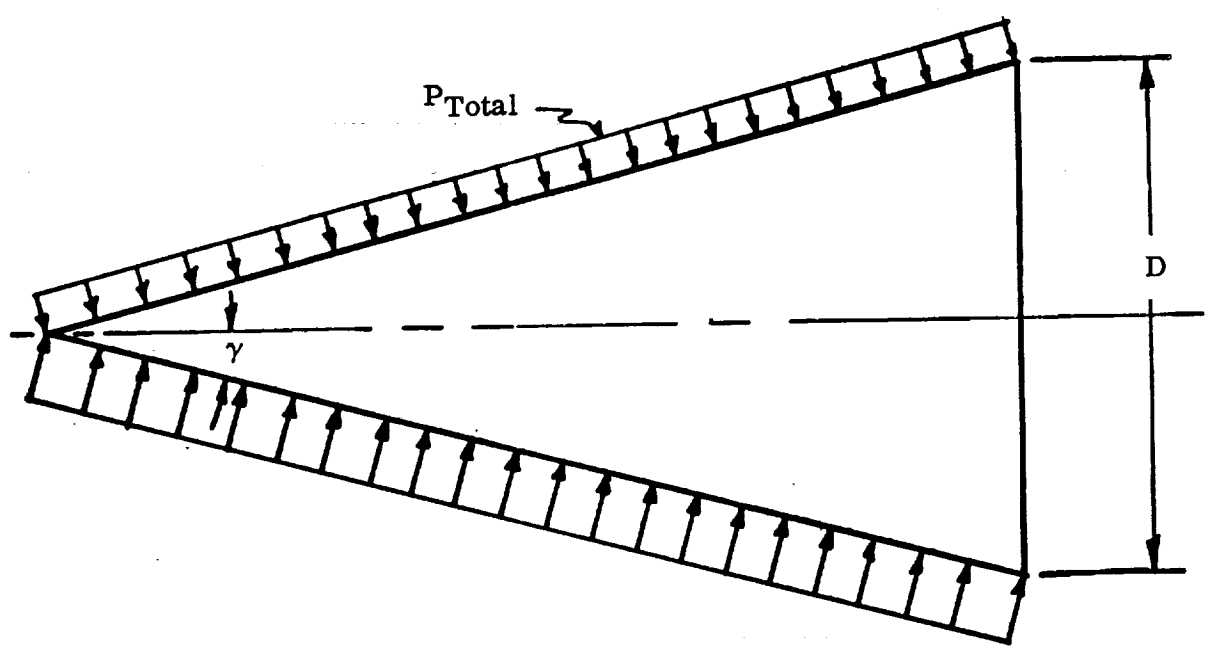
where  $\eta$  represents the factor of safety (1.4 for this study),  $q$  the dynamic pressure, and  $\left[ \frac{dC_x}{d(x/D)} \right]_o$  and  $\left[ \frac{dC_{z\alpha}}{d(x/D)} \right]_o$  represent the axial and normal force distribution coefficients, respectively, at  $x/D = 0$ . A typical variation of the pressure around the periphery of the cone is shown in Figure 2. Also in Appendix A, the derivations for the skin loading in pounds per inch of circumference at any station may be found for the axial load (Equation 2) and the bending load (Equation 3).

$$N_A = q \frac{L}{8} \left[ \frac{dC_x}{d(x/D)} \right]_o \quad (2)$$

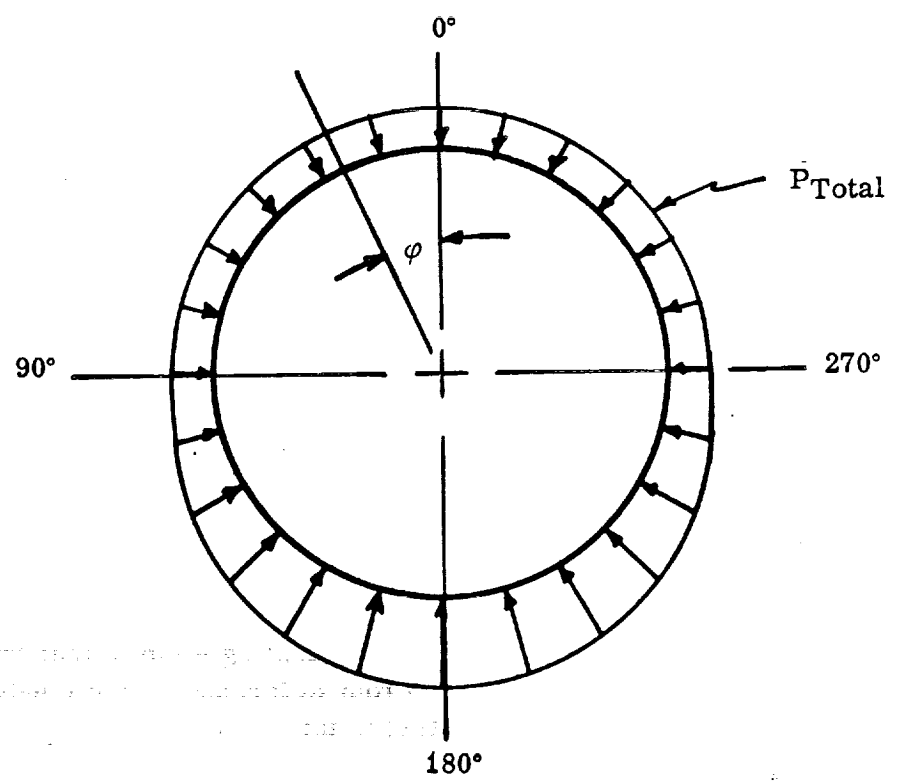
$$N_B = q \frac{\alpha L}{12 \tan \gamma} \left[ \frac{dC_{z\alpha}}{d(x/D)} \right]_o \cos \varphi \quad (3)$$

When a cone is subjected to an external pressure, stability under the resultant compressive loads is the primary problem in structural analysis. Three possible types of instability were investigated, namely: panel instability; stability of the stiffening ring; and general, or overall, instability of the cone. For each stability consideration, primary expressions used and reference to their derivation, or origin, are contained herein for the reader's information.





A. Longitudinal Variation



B. Circumferential Variation

FIGURE 2. TYPICAL PRESSURE VARIATION FOR EQUATION (1), WITH ANGLE OF ATTACK,  $\alpha$

The stability of a truncated conical shell ("panel" stability) that is subjected to an external pressure was investigated in Reference (5). The critical buckling pressure,  $P_{CR}$ , was empirically determined for the customary range of conical shell configurations as:

$$P_{CR} = \frac{K_1 \tan \gamma}{\left(\frac{a_n}{\cos \gamma}\right)^{5/2}} \frac{E (h)^{5/2}}{[1 + \bar{\theta} (\lambda - 0.5)]} \quad (4)$$

In addition to the variables in Equation 4 which are defined by Figures 1 and 3, the parameters  $K_1$ ,  $\bar{\theta}$ , and  $\lambda$  depend upon geometric and stress relationships. The range in which the  $P_{CR}$  solution is considered valid (Reference 5) is indicated by expression (5):

$$0.49 > (1 - 2 \lambda) \bar{\theta} > -0.83 \quad (5)$$

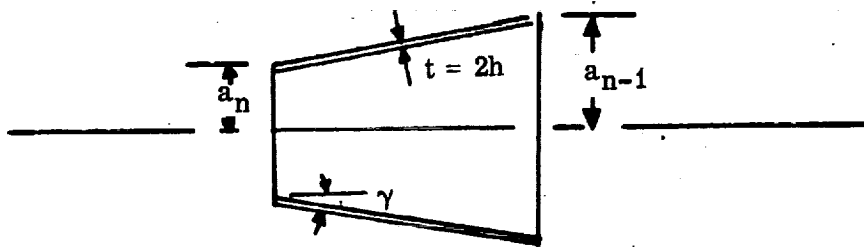


FIGURE 3. SECTION THROUGH CONICAL SHELL FRUSTUM

After satisfying the stability of the conical shell frustrum, stiffening rings must be inserted that will limit the shell buckling wave to that frustrum, or bay, i. e., control "general" instability. From Reference 6, the length of shell, between rings, that will limit local buckling to the bay in question may be expressed as:

$$l = \frac{4\sqrt{t a_n}}{\sqrt{\cos \gamma} \sqrt{3(1 - \sqrt{2})}} \quad (6)$$

Additionally from Reference 6, an equation for the reactive force on ring stiffeners in a semi-monocoque cone subjected to external pressure was obtained which would permit their analysis. After several modes of failure were investigated, the ring requirement for general stability was found to govern the ring design. Consequently, the cylindrical general stability equation presented in Reference 7 was modified for cones and is expressed in the required moment-of-inertia form as:

$$I_{\text{req}} = l \left( \frac{a_n}{\cos \gamma} \right)^2 \left( \frac{1}{t} \right)^{1/3} \left( \frac{P_{\text{cr}} D}{11.02 E \tan \gamma} \right)^{4/3} \quad (7)$$

Discontinuity stresses in the shell near the rings, although not affecting stability, may be critical and were checked by equations developed in Reference 6. Upon using the notations in this MTP, the axial and hoop stress, respectively, become

$$\sigma_{\text{CA}} = \frac{N_B + N_A}{t \cos \gamma}, \text{ and} \quad (8)$$

$$\sigma_{\text{CH}} = \frac{P_o}{t \cos \gamma} \left[ l + \frac{\sqrt{\sin \gamma}}{2} + a_n \left( 1 + \frac{\bar{\lambda} \sqrt{\cos \gamma}}{2} \right) \right] \quad (9)$$

As a result of the various parameters and dependent expressions evidenced in the preceding paragraphs, proportions cannot be determined directly for a cone nor any short conical frustum. A trial and error procedure must be used to determine the shell thickness at any point for a given spacing of the rings. Upon recalling the minimum weight condition established in the beginning, one would surmise that a uniformly varying (tapered between the base and apex) shell thickness with variable ring spacing would produce this desired result. Since this approach would not be practical in monocoque construction, a stepped-down skin thickness with variable stiffener ring spacings was chosen as the best approximation.

The design of these "steps", or bays, consisted of the design of short conical shell frustums bounded by stiffening rings. This type design, hereafter referred to as the "variable skin thickness" approach, employed standard gage variations in skin thicknesses with conventional proportions for ring cross sections. The minimum skin thickness throughout the program was held at .030 inches. The shells were designed to withstand the calculated pressure at the design point and the bay length was determined by minimum weight procedures which are explained in detail in a later paragraph. For comparison purposes, a constant thickness shell with the necessary ring reinforcement for buckling was also proportioned.

The stiffening ring cross sections were determined by a general relationship of  $I_{req}$  to  $AR^2$ . The typical cross section chosen for both the aluminum alloy and fiberglass is shown in Figure 4.

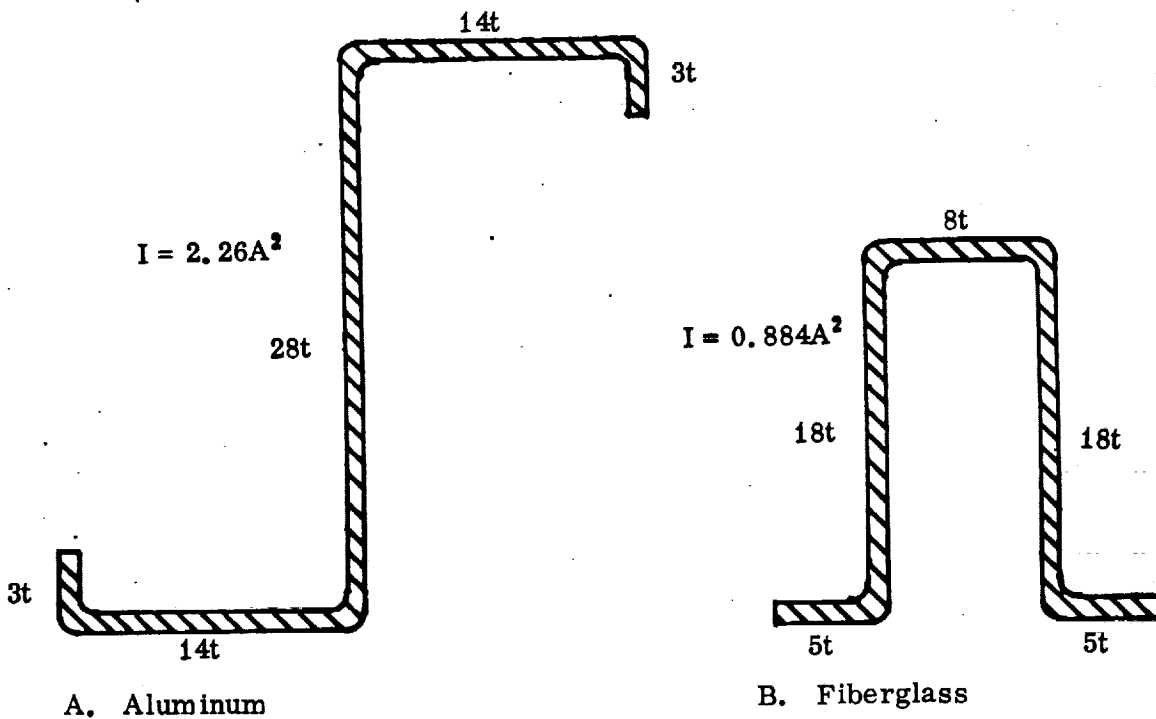


FIGURE 4. TYPICAL RING STIFFENER CROSS SECTIONS

The design procedure was applied to four typical upper stage vehicle diameters to obtain an optimum cone for each. The diameters that were chosen are: 120", 154", 220", and 260". With the cone base diameter remaining a constant, the shell slope was changed by varying the internal cone half angle. This angle assumed the following values: 10°, 13.322°, 15°, 20°, 25°, and 30°. In addition to the variable cone angle, two separate materials were considered, those being (1) aluminum alloy, and (2) glass-fiber-reinforced, silicone laminate (fiberglass).

Consideration of all the above mentioned variables made it necessary to investigate 144 separate nose cones. The numerous trials involved to obtain the optimum for each cone prompted the use of an electronic computer. By using basic geometry and the aforementioned procedure of analysis, a computer program was written to make the trial and error weight optimization of the various cones.

The operations of the computer program will be explained in a general manner by outlining the steps taken to optimize the nose cones. The program progressed from the base diameter to the apex as short conical frustums were designed for the critical condition. The shortest permissible stiffening-ring spacing, with a minimum limit of four inches, that would satisfy the range test of Expression 5, or that would prevent ring deformation from affecting stability of adjacent rings, was determined for the particular cone station in question. The skin thickness for this bay was found by starting at the minimum of .030 inch and incrementing in standard gage steps until the critical buckling pressure exceeded the applied pressure. The required ring size was then calculated for this combination of minimum spacing and skin thickness, and the weight per longitudinal running inch was determined and stored.

Keeping the skin thickness constant, this minimum spacing was then incrementally increased, a new ring size was determined, and the corresponding weight calculation was again made. This spacing incrementation continued until a greater skin thickness was necessary to meet the critical buckling pressure requirement. Then the weights for each of these spacings were compared to obtain a minimum. The corresponding spacing, skin thickness, and ring area were considered optimum at the specific cone location. The investigation was moved to a new reference and the corresponding optimum bay determined. These optimum bays were then united and the weights summed to produce a nose cone design which was considered optimum.

The total weight of the cones for a particular base diameter and material were plotted as a function of the cone half angle. These curves made possible the comparison of materials and cone angles with respect to weight. Curves of the weight per unit volume versus cone half angle were also prepared to show its variation.

## B. BLUNTED CONE ANALYSIS

The variation in weight due to blunting of the nose cone was also investigated. Blunting, even though a relatively smooth fairing such as a hemispherical nose cap is affixed to the end, causes a significant change in pressure variation near the forward end. Aft of this nose cap the pressure variation remains essentially the same as that in the sharp cone. A general blunted cone schematic and a typical pressure loading curve -- derived from the aeroballistic data of Appendix B for a cone half angle of  $13.322^\circ$  -- are shown in Figure 5. Also, Figure 5-B exhibits the relatively close approximation by a cosine function of the actual pressure loading. This approximation makes possible a general solution for a nose cap of any diameter (d).

General solutions for the meridional and hoop stress in the nose cap with the cosine loading of Figure 5-B were developed by Mr. J. N. Nunnery of M-P&VE-SS and are shown as Equations 10 and 11, respectively.

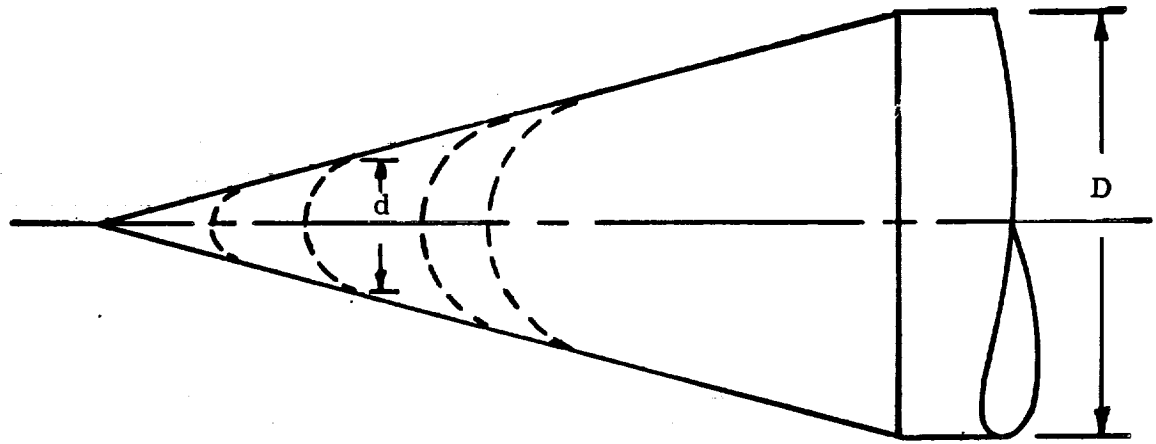
$$N_\phi = -\frac{DC}{2 \sin^2 \phi_2} \left[ \frac{\cos^3 \phi_2}{3} - \frac{1}{3} \right] \quad (10)$$

$$N_\theta = -N_\phi + \frac{DC}{2} \cos \phi_2 \quad (11)$$

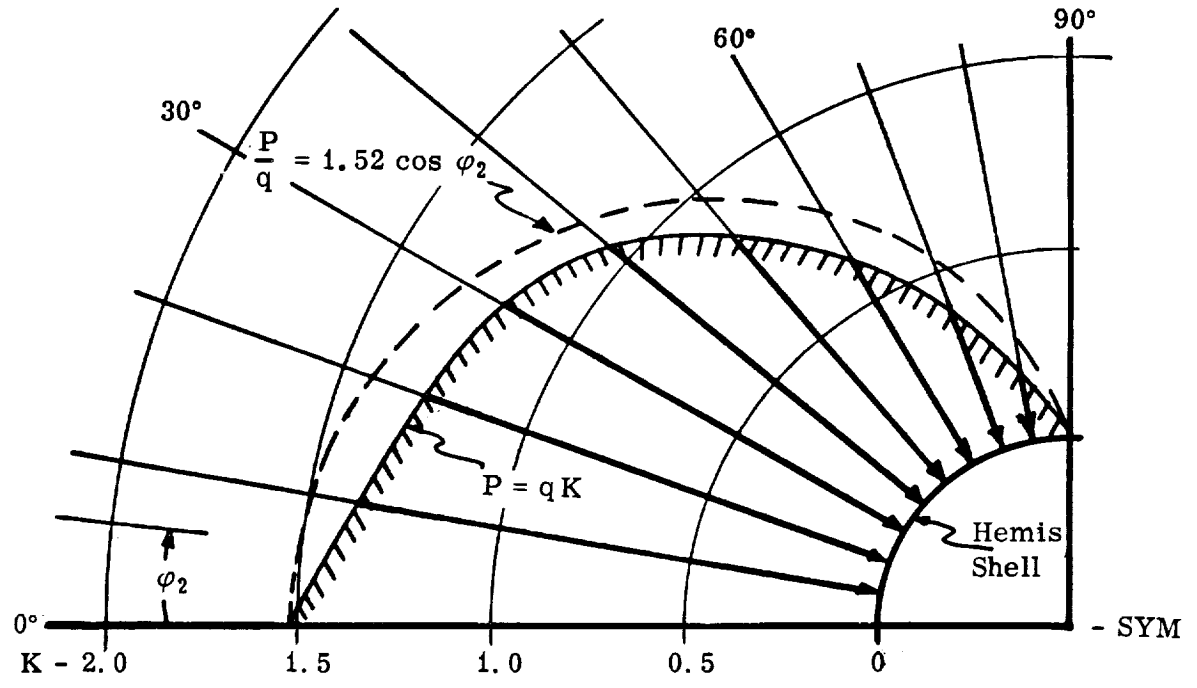
The nose cap thickness was determined by use of the above stress equations and the following relation:

$$\sigma_{CR} = 0.25E \frac{t \cdot 2}{D} \quad (12)$$

The remainder of the nose cone -- the conical portion between the nose cap and the base diameter -- was proportioned in an identical manner to the sharp cone analysis procedure. The total weight of the combined segments was then determined for the particular d/D ratio.



A. Blunted Cone Schematic



B. Pressure Variation; D = 260"

FIGURE 5. BLUNTED CONE SCHEMATIC AND PRESSURE VARIATION ON HEMISPHERICAL SHELL

Weights were evaluated for a full range of bluntness ratios ( $d/D$ ) using an aluminum alloy cone with base diameter of 260 inches and cone half angle of  $13.322^\circ$ , the only cone angle for which necessary pressure data was available. The total blunted cone weight was plotted as a function of  $d/D$  for nose coverings ranging from a simple hemisphere to a full cone.

### C. RESULTS

The resulting system obtained under the analysis presented was a monocoque cone with a series of constant gage frustums. Within a frustum of a particular skin gage, there was a close ring spacing at the large end and generally increased spacing towards the smaller radii, a spacing roughly inversely proportional to the local average radius. A typical result is presented in Figure 6 and Table I to illustrate this trend.

The weights presented in the curves should be quite accurate for the specified conditions. Although weights of skin splices and joints were not computed, an investigation into the magnitude of these weights proved them to be negligible, particularly for welded connections. Weights of frame splices were adequately compensated for by using the contour radius at the frame station in lieu of the radius to the centroid of the ring cross section.

The calculated points defining the curves generally follow a smooth parabolic curve; however, some scatter may be observed in a few of the curves. This divergence is attributed to the restriction to standard skin thicknesses and the limitation of a minimum skin thickness.

Figures 7 through 10 show the plot of total cone weight versus cone half angle for aluminum cones of the various diameters and their associated dynamic pressures. Each of these curves represents cones of standard gage skins and conventionally proportioned rings of standard gage material (See Figure 4-A).

Figure 11 exhibits the weight variation of cones having the same skin gage throughout the cone length and conventionally proportioned rings. The skin gage is determined by the bay with the largest average radius and is referred to as uniform skin thickness condition.

A typical variation in weight for glass-fiber reinforced, silicone resin, laminated cones is shown in Figure 12. This curve presents cones that utilize a one-hundredth-inch incremental variation in skin thickness between rings and having ring proportions as shown in Figure 4-B.



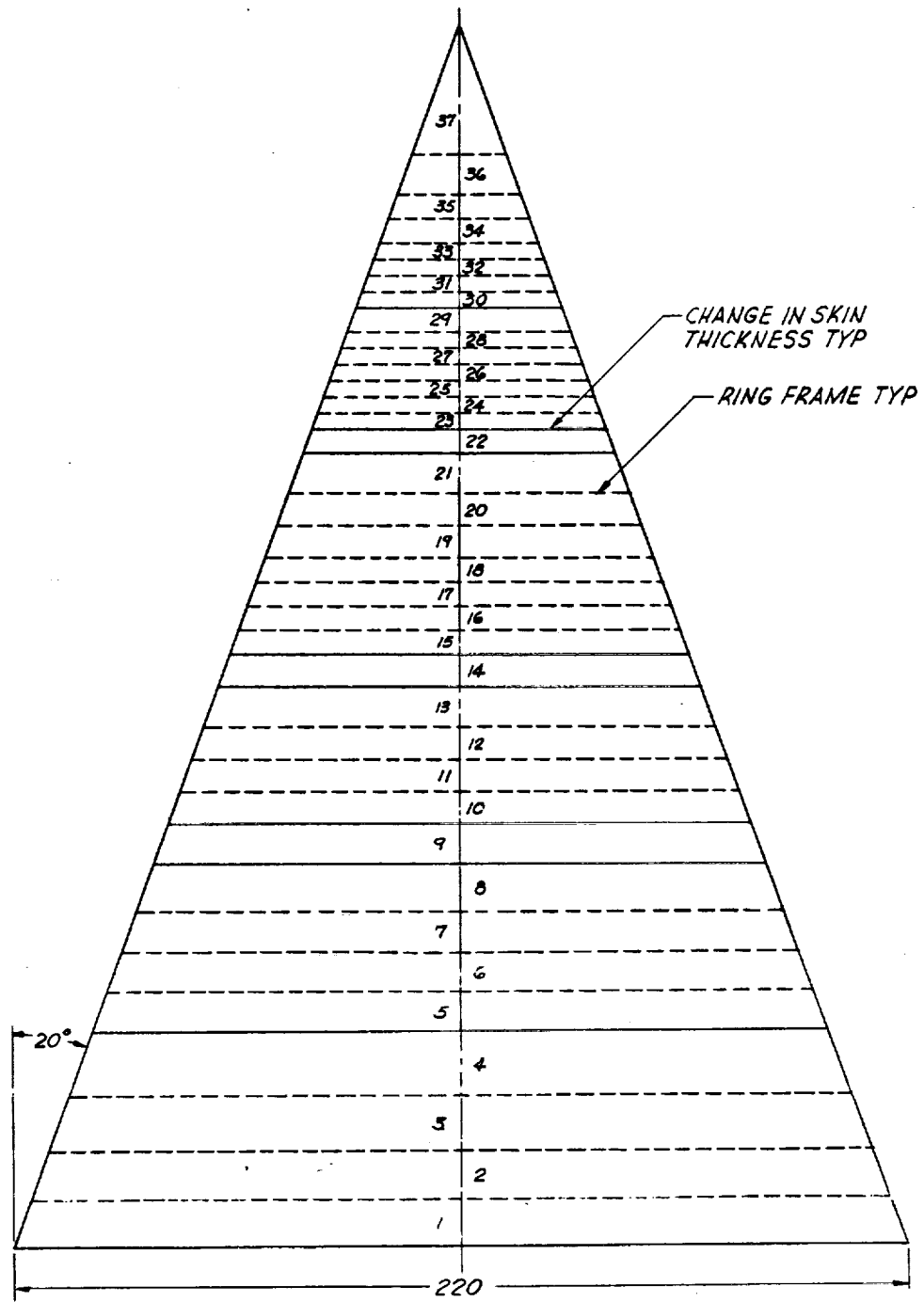


FIGURE 6. SCHEMATIC OF TYPICAL FINAL DESIGN

TABLE I

## STRUCTURAL TABULATIONS FOR FIGURE 6

<u>Bay No.</u>	<u>Bay Length</u>	<u>Skin Thickness</u>	<u>Forward Ring Area</u>	<u>Minimum Weight Per Inch</u>
1	12	.125	.3125	10.74
2	12	.125	.2461	9.95
3	14	.125	.2461	9.31
4	16	.125	.2461	8.67
5	10	.100	.2461	7.26
6	10	.100	.2461	6.96
7	10	.100	.2461	6.66
8	12	.100	.2461	6.13
9	10	.090	.2461	5.51
10	8	.080	.1550	4.58
11	8	.080	.1550	4.39
12	8	.080	.1550	4.19
13	10	.080	.1550	3.83
14	8	.071	.1550	3.42
15	6	.063	.1550	3.19
16	6	.063	.0992	2.76
17	6	.063	.0992	2.65
18	6	.063	.0992	2.53
19	8	.063	.0992	2.28
20	8	.063	.0992	2.14
21	10	.063	.0992	1.91
22	6	.050	.0992	1.60
23	4	.040	.0635	1.28
24	4	.040	.0635	1.23
25	4	.040	.0635	1.17
26	4	.040	.0635	1.12
27	4	.040	.0635	1.06
28	4	.040	.0635	1.01
29	6	.040	.0635	0.86
30	4	.032	.0635	0.75
31	4	.032	.0635	0.70
32	4	.032	.0635	0.66
33	4	.032	.0635	0.61
34	6	.032	.0635	0.50
35	6	.032	.0635	0.43
36	10	.032	.0635	0.32

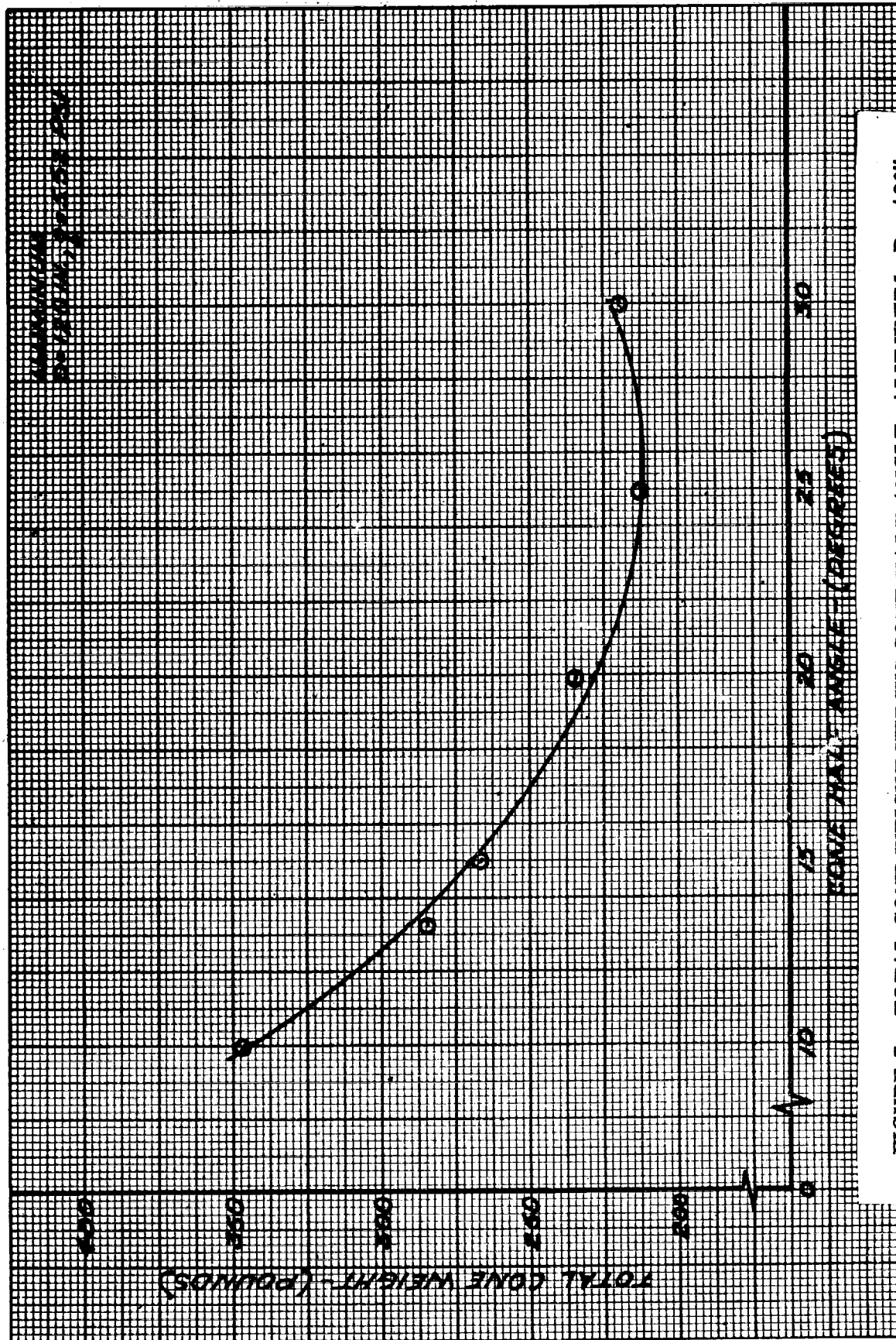


FIGURE 7. TOTAL CONE WEIGHT VERSUS CONE HALF ANGLE; ALUMINUM, D = 120"

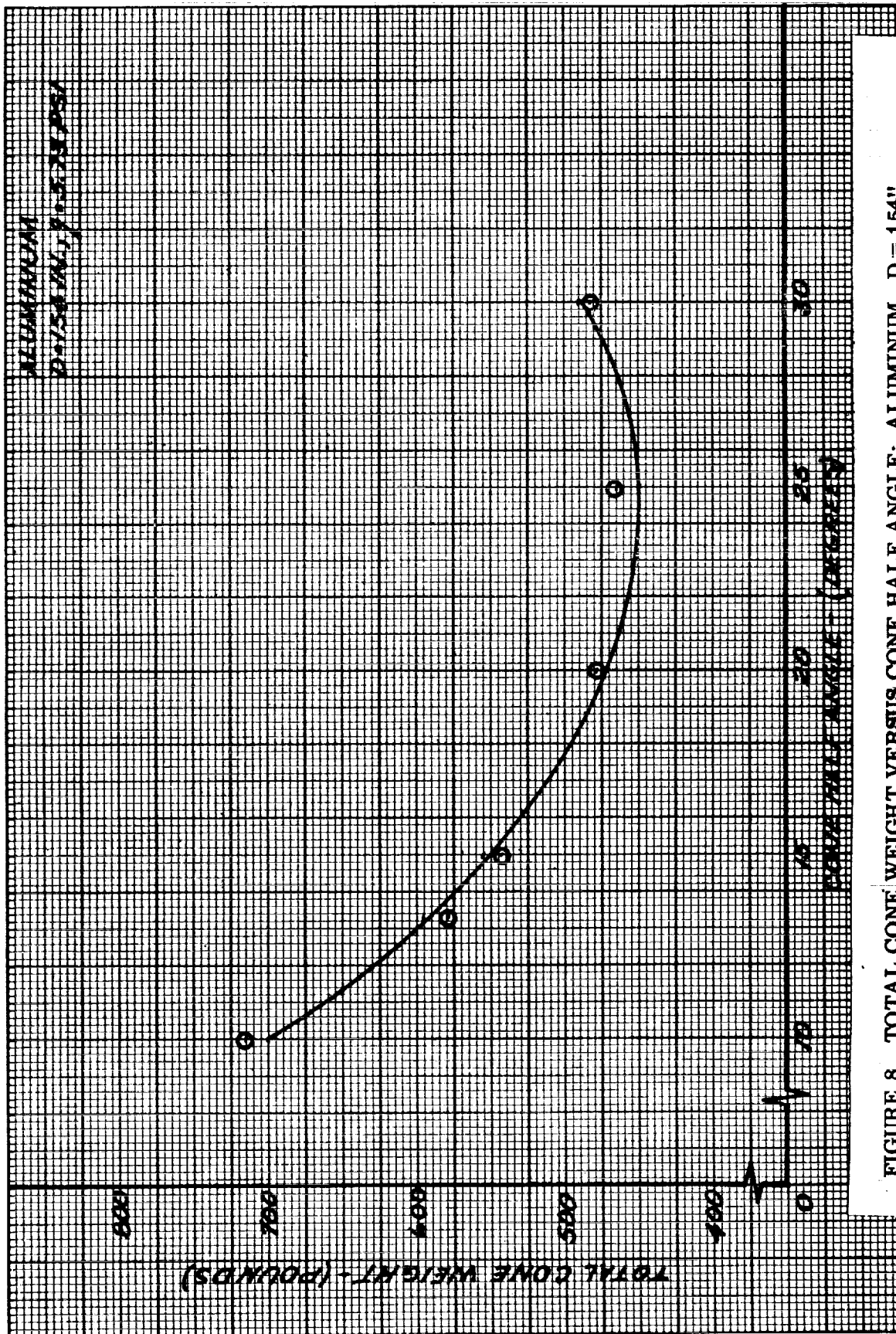


FIGURE 8. TOTAL CONE WEIGHT VERSUS CONE HALF ANGLE; ALUMINUM, D = 154"

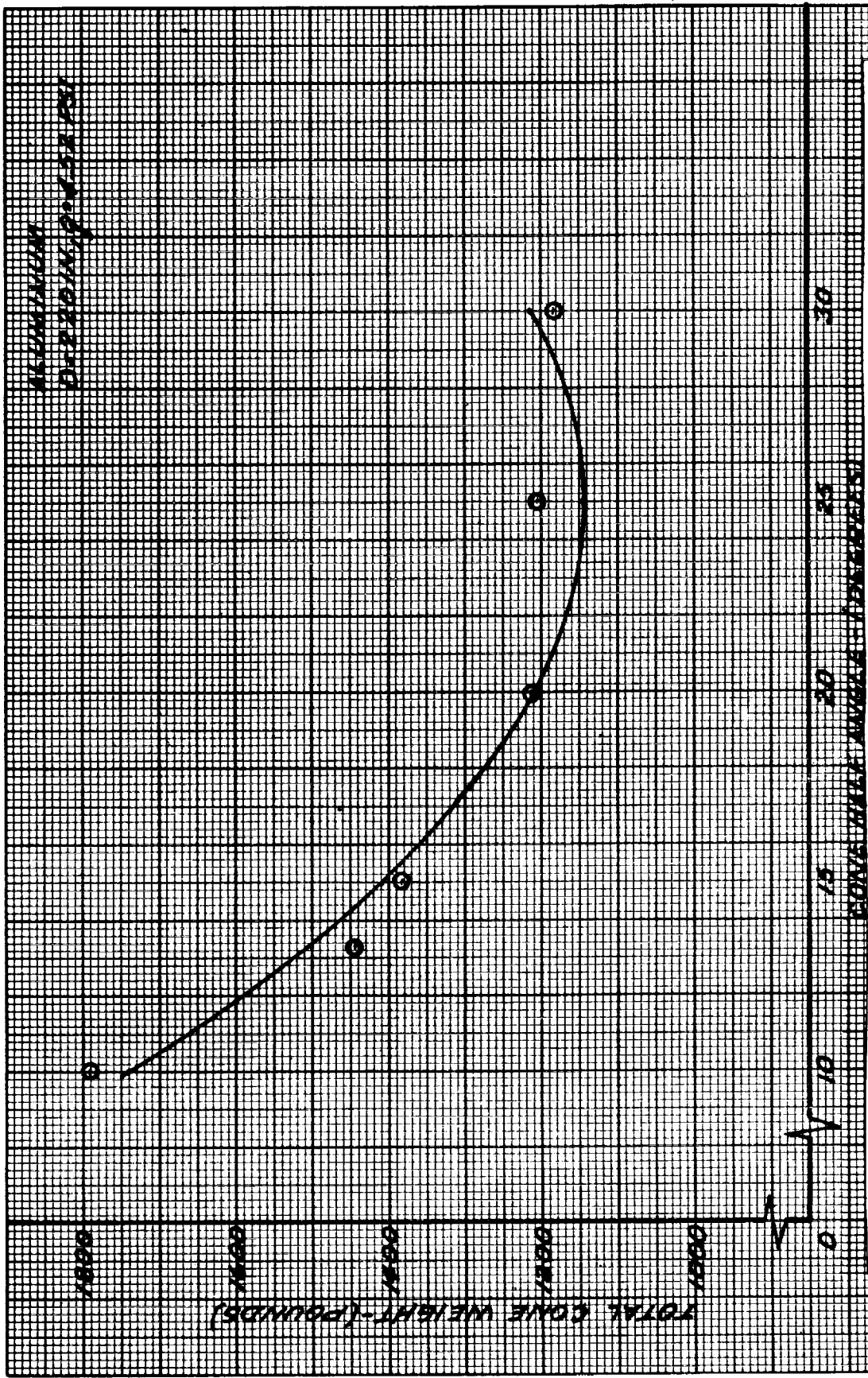


FIGURE 9. TOTAL CONE WEIGHT VERSUS CONE HALF ANGLE: ALUMINUM, D = 220"

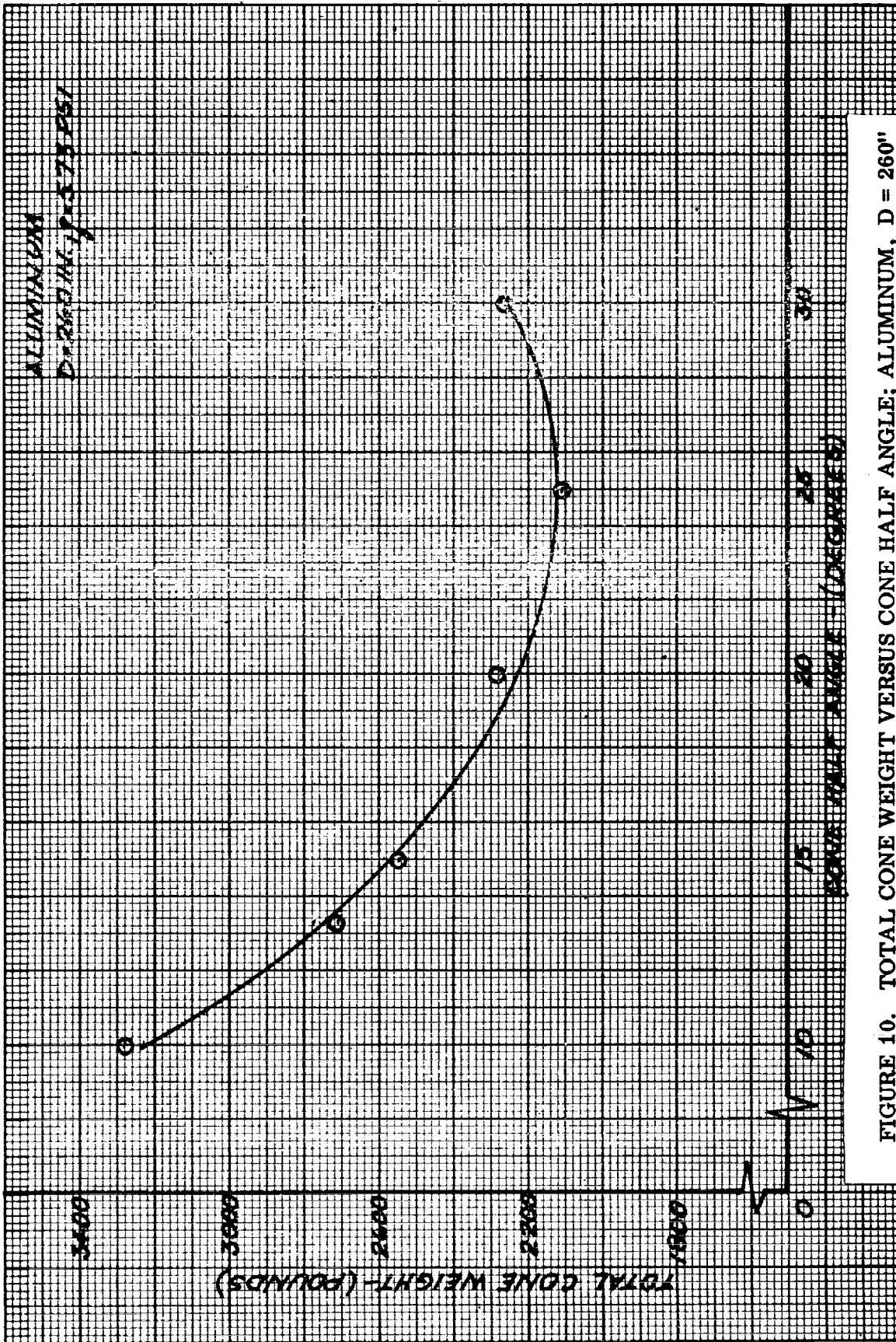


FIGURE 10. TOTAL CONE WEIGHT VERSUS CONE HALF ANGLE; ALUMINUM, D = 260"



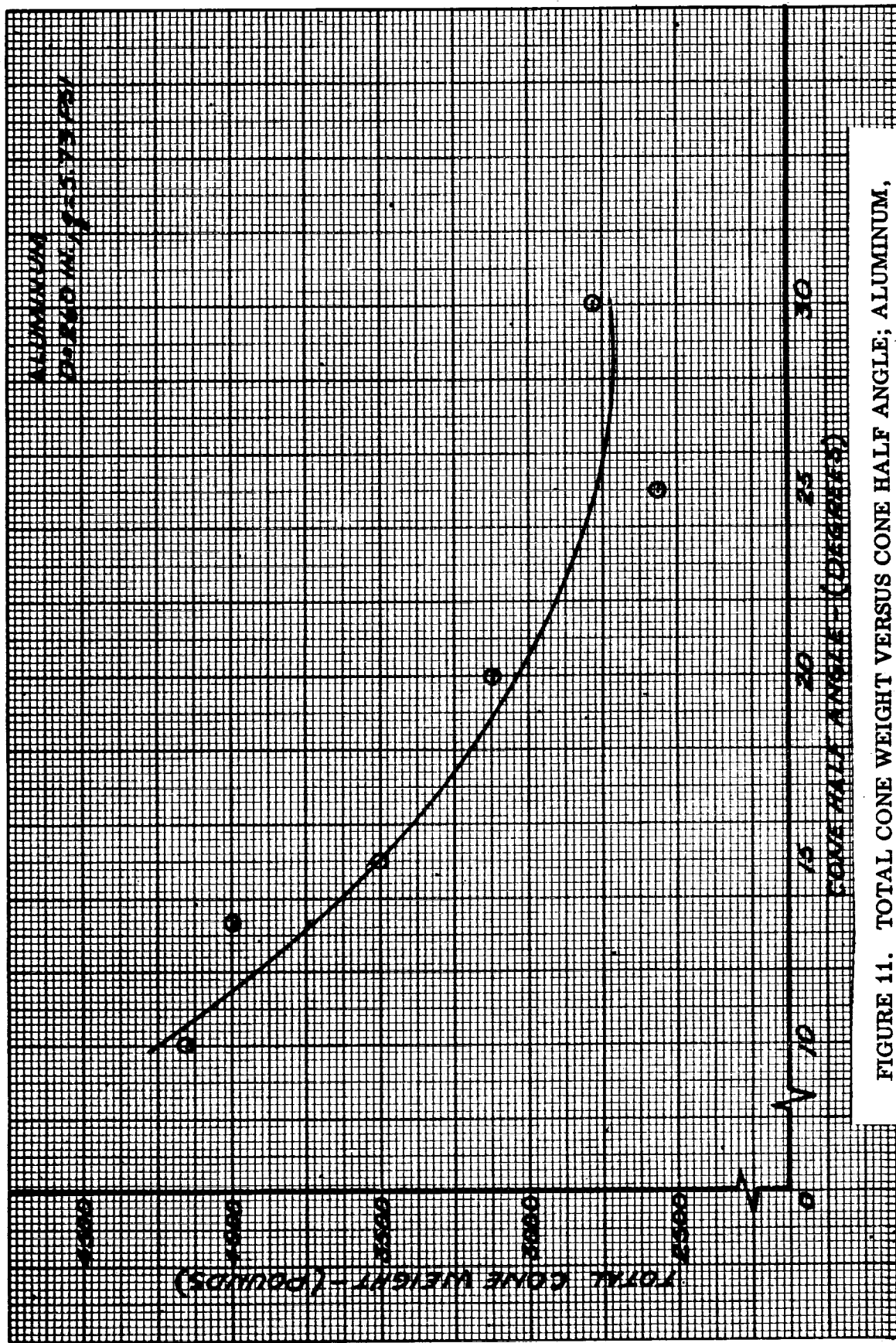


FIGURE 11. TOTAL CONE WEIGHT VERSUS CONE HALF ANGLE; ALUMINUM,  
UNIFORM SKIN THICKNESS, D = 260"

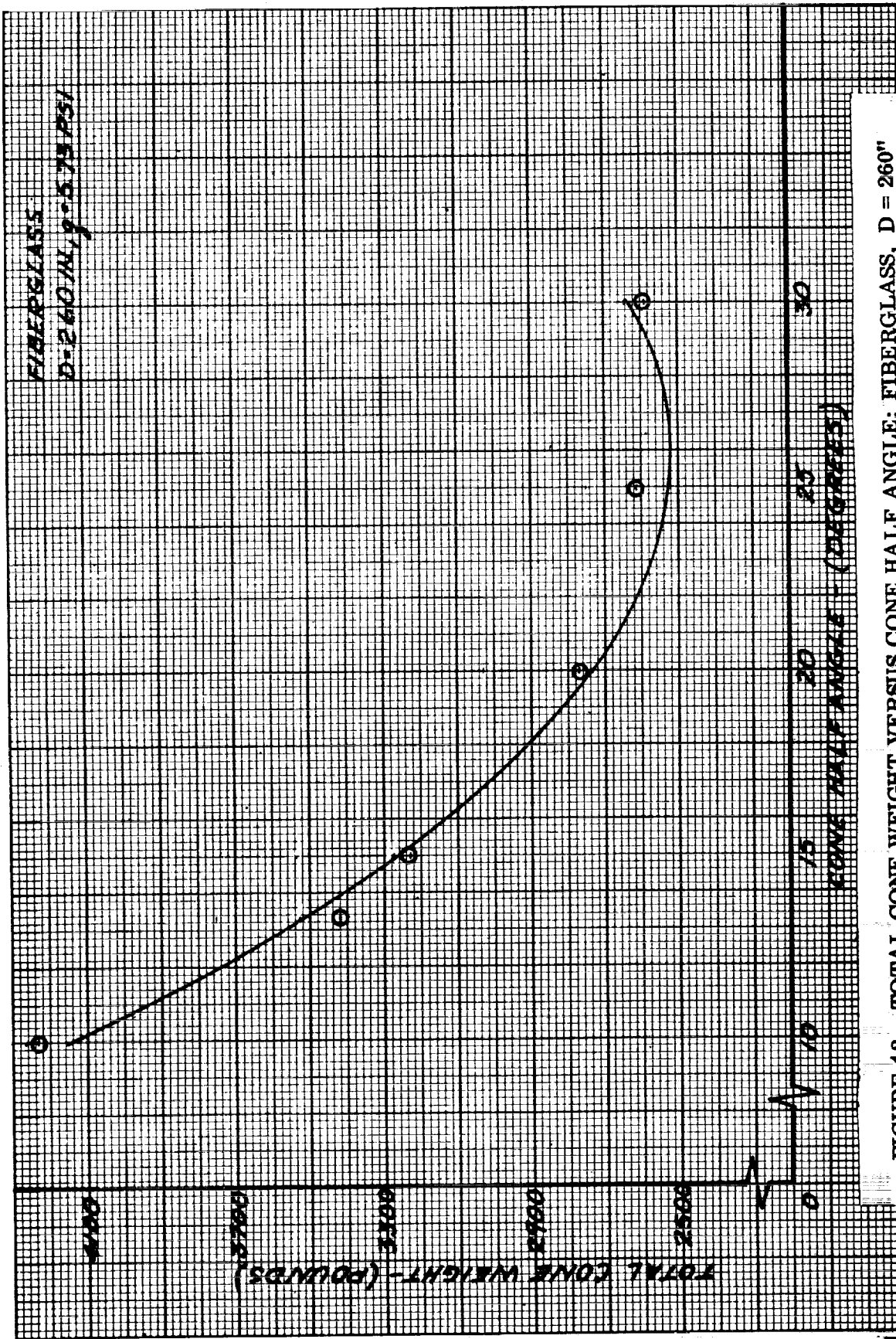


FIGURE 12. TOTAL CONE WEIGHT VERSUS CONE HALF ANGLE; FIBERGLASS, D = 260"



Figure 13 is a comparison of Figures 10 and 11. The cones of Figure 10 make use of standard gage skins in a "stepped" variation while the uniform skin thickness case is presented in Figure 11.

Figure 14 shows a comparison of the curves of Figures 10 and 12 (aluminum vs. fiberglass). This comparison may be considered valid if there is the reasonable assumption that minor differences would occur in connection weight.

The variation of weight with cone half angle for a 220-inch base diameter cone over a reasonable range of dynamic pressures is exhibited in Figure 15. To account for point scatter these curves were "best-fitted" with a second degree curve by a computer program.

Figure 16 shows the variation in cone weight per unit enclosed volume for aluminum cones of all the various half-angles. Here again, this data is limited to results obtained for standard gage skins and conventionally proportioned rings. This band is representative of all cones subjected to a dynamic pressure of 5.52 to 5.73 psi. The trajectory used for the 220-inch diameter cone resulted in a somewhat lower dynamic pressure and the resultant cone weights fall below the band shown.

The final curve, Figure 17, is presented to indicate the structural weight variation with the bluntness ratio. This curve was obtained for a cone with a  $13.322^\circ$  half angle, but the trend should not vary significantly in the range of half-angles considered in this report.

#### D. INTERPRETATION OF RESULTS

The results of this study, as presented graphically herein, have revealed some interesting points concerning nose cone design.

Possibly of foremost interest was the close ring spacing obtained for optimum weight designs. This represents a departure from the general cylindrical structure design used in typical rocket vehicles and results from the overwhelming influence of the circumferential pressure, or hoop compression, stability requirement on skin gages.

Another result clearly seen is that a minimum weight cone for any diameter, or material, falls very closely to a  $25^\circ$  half angle design. This is purely from a structural weight point of view, of course, and does not consider down-stream buffeting effects. This angle, however, should provide a starting point for nose cones utilizing ogive or modified ogive (including conically-segmented) cones.

A look at Figure 14 shows the obvious superiority of aluminum over fiberglass construction for this application. An explanation for this superiority is given in equation 4, which is repeated below.

$$P_{CR} = \frac{K_1 \tan \gamma}{\left(\frac{-a_n}{\cos \gamma}\right)^{5/2}} \frac{E (h)^{5/2}}{[1 + \bar{\theta} (\lambda - 0.5)]}$$

For a given  $\gamma$ , and assuming everything constant in this equation but  $h$  and  $E$ , an assumption not significantly in error for most cases, the critical pressure may be expressed by:

$$P_{CR} = (\text{constant}) E (h)^{5/2}$$

Inserting the appropriate values for aluminum and fiberglass will then show the trend illustrated in Figure 14. This weight difference could conceivably be altered significantly, however, when effects of aerodynamic heating are included. The heat transfer characteristics of fiberglass and aluminum are vastly different and cannot be ignored in the final analysis of candidate materials.

The most useful information derived from this program may well be illustrated by the curves of Figures 15 and 16. Figure 16 shows that the weight per unit volume is essentially constant for an aluminum cone having a particular cone angle, dynamic pressure of 5.6 psi, and maximum angle of attack of 7°. Then, if these conditions are met, a close estimate of the nose cone weight for any base diameter within the range studied may be made from this figure. Furthermore, assuming this relationship exists for reasonable dynamic pressure ranges, use of Figure 15 would allow a weight estimate for cones subjected to dynamic pressures of 3 to 7 psi and an angle-of-attack of 7°. This assumption of a constant weight-per-unit-volume curve should produce reasonably accurate weight estimates.

Lastly, the bluntness variation study performed on the 13.322° half angle cone has shown a weight reduction may be obtained through blunting of cones. Here again, an aerodynamic buffeting problem exists for large bluntness ratios. Caution must, therefore, be used in considering this means of potential weight saving.

## CONCLUSIONS

Since this study ignores effects of aerodynamic heating and buffeting, the conclusions drawn from it, alone, must necessarily be limited. However, this investigation has provided several indicators for determining the lightest weight nose cones. Disregarding the effects of buffeting and heating, the minimum weight cone will be provided by:

1. Using a 25° half angle cone,
2. Blunting the cone as much as possible
3. Using an aluminum alloy in lieu of fiberglass.

In addition, it may be concluded that the weight per unit enclosed volume is a fixed quantity when the maximum dynamic pressure, maximum angle of attack, and nose cone angle are held constant. By adopting this premise, and by using Figures 15 and 16, the weight of a sharp nosed cone of given geometry may be accurately predicted when the maximum angle of attack and maximum dynamic pressure are known.

Further, since aeroballistic considerations discourage the use of a 25° half angle nose cone, a composite shape should be derived to restrict the angular difference between any two intersecting surfaces to a small angle. This shape, apparently, would originate with a 25° half angle blunted cone and be of such configuration that buffeting would not occur aft of the cylinder junction. This could be accomplished by either fairing the cone and cylinder with an ogive section or by insertion of a conical frustum with a smaller half angle. The latter approach appears more desirable from manufacturing considerations and this configuration is recommended for initial study. There is the anticipation that this new shape will exhibit improvement in total nose cone weight, weight to unit-enclosed-volume ratio, and weight to aerodynamic drag ratio over those of the sharp-nosed cone.

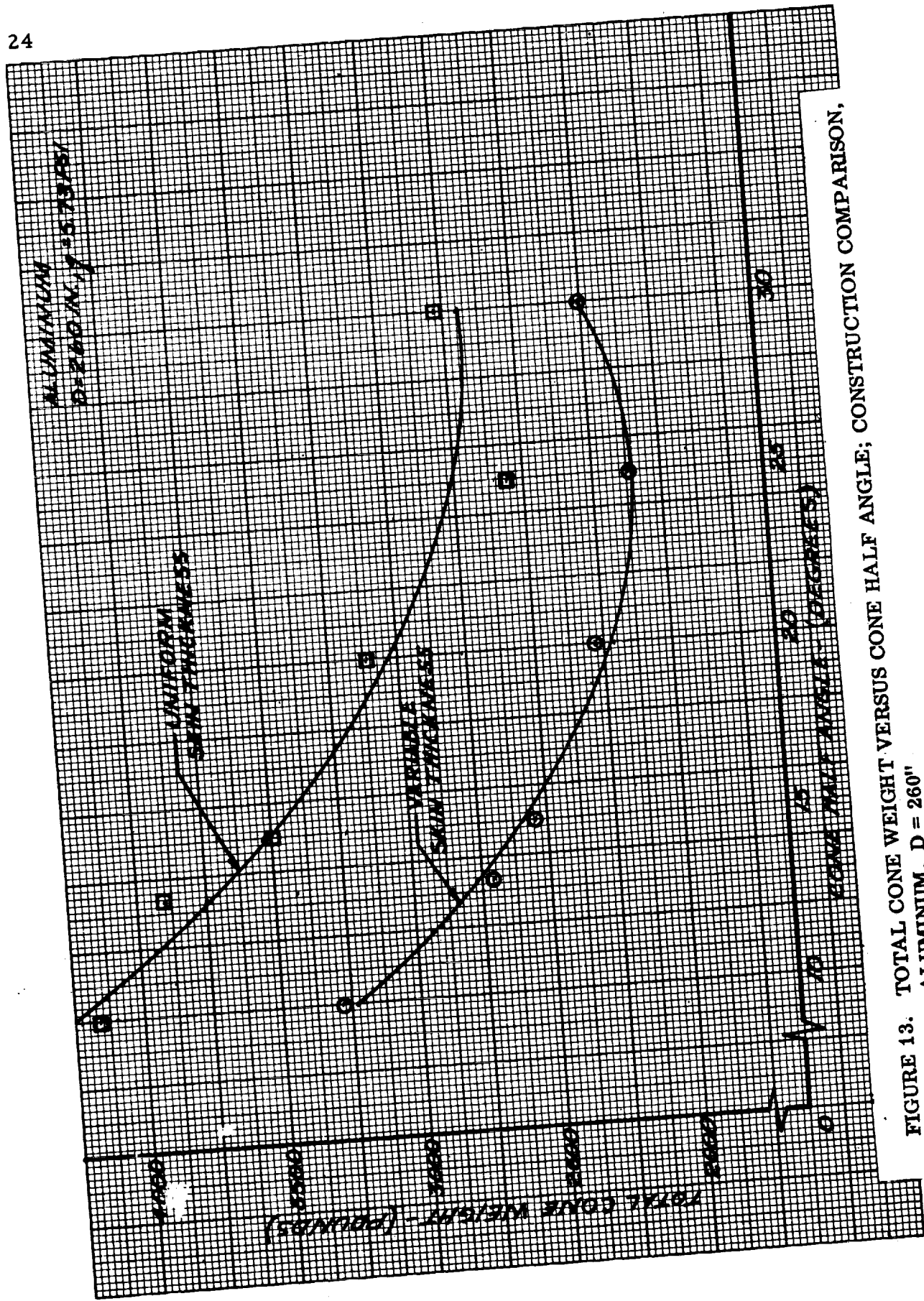


FIGURE 13. TOTAL CONE WEIGHT VERSUS CONE HALF ANGLE; CONSTRUCTION COMPARISON, ALUMINUM, D = 260"

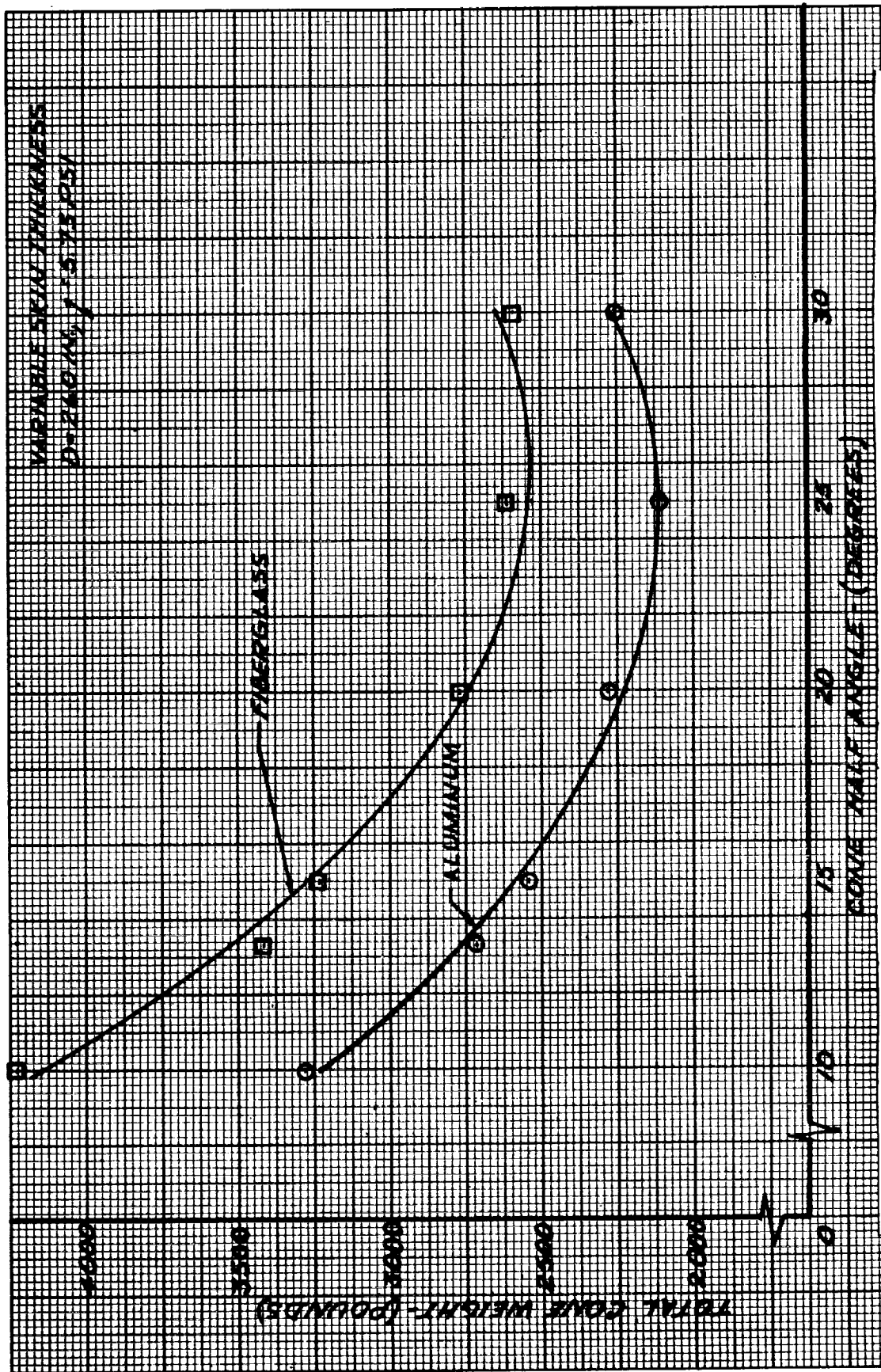


FIGURE 14. TOTAL CONE WEIGHT VERSUS CONE HALF ANGLE; ALUMINUM - FIBERGLASS COMPARISON, D = 260"

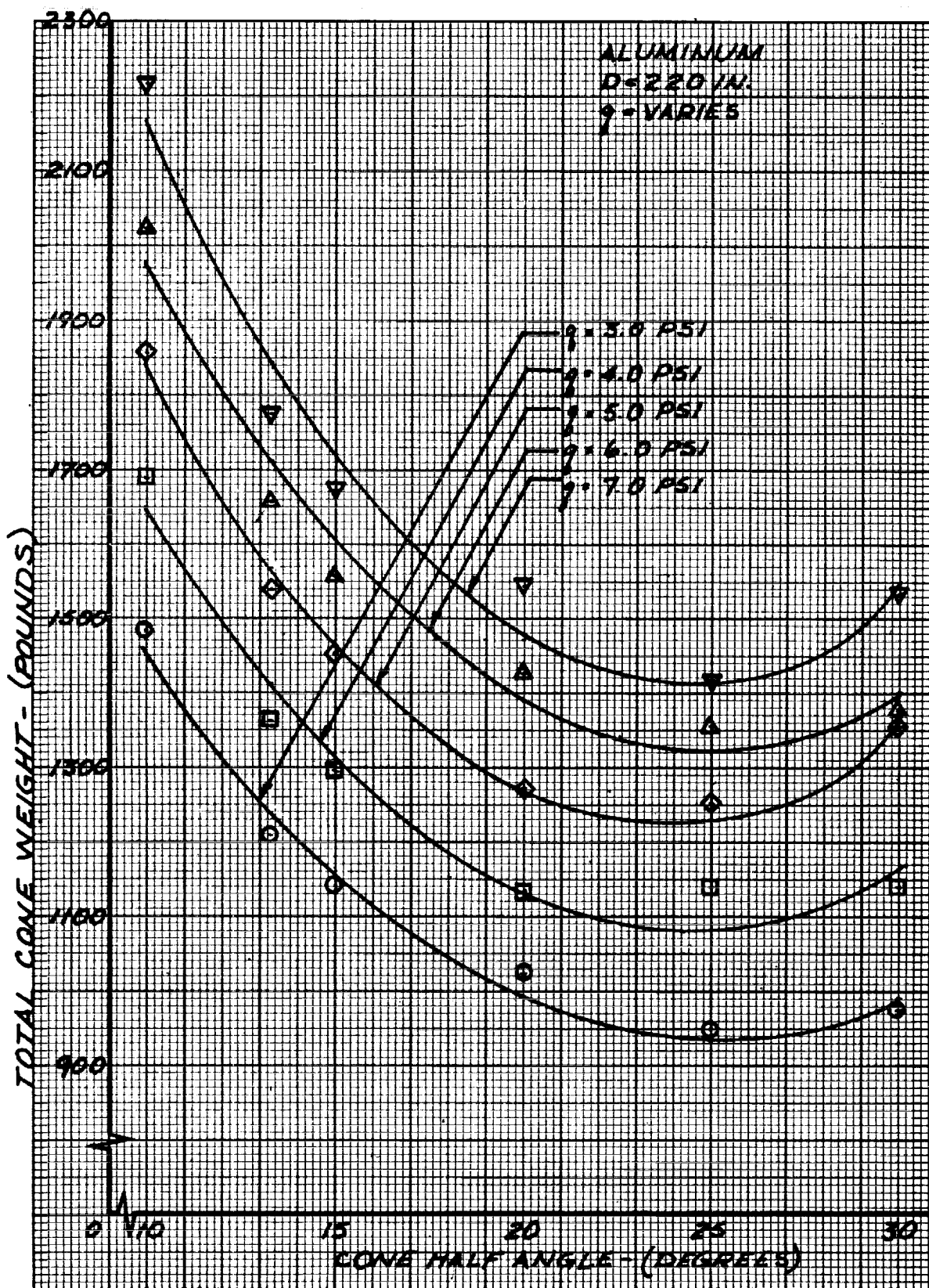


FIGURE 15. TOTAL CONE WEIGHT VERSUS CONE HALF ANGLE; ALUMINUM; q COMPARISON, D = 220"



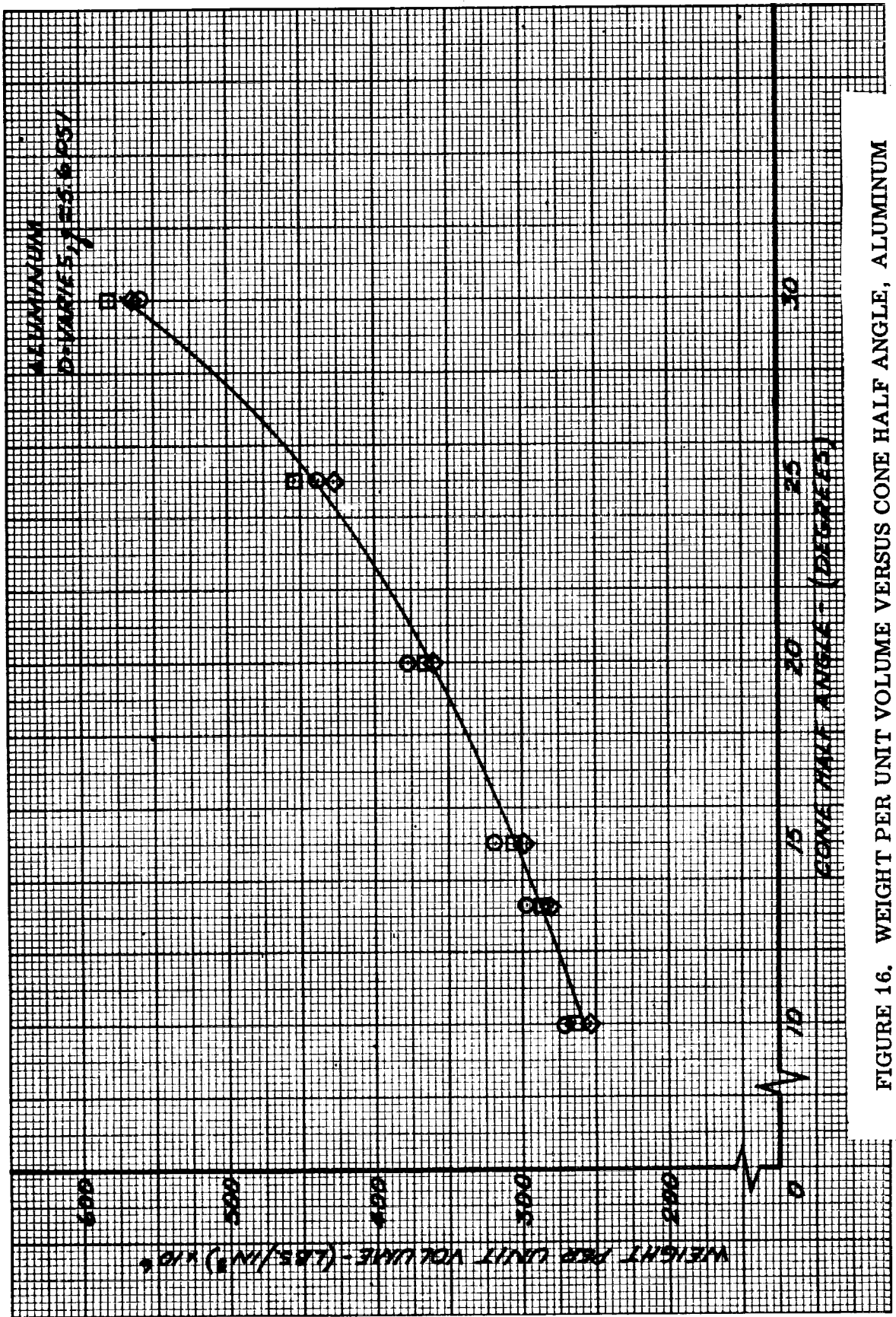


FIGURE 16. WEIGHT PER UNIT VOLUME VERSUS CONE HALF ANGLE, ALUMINUM  
q = 5.6 psi

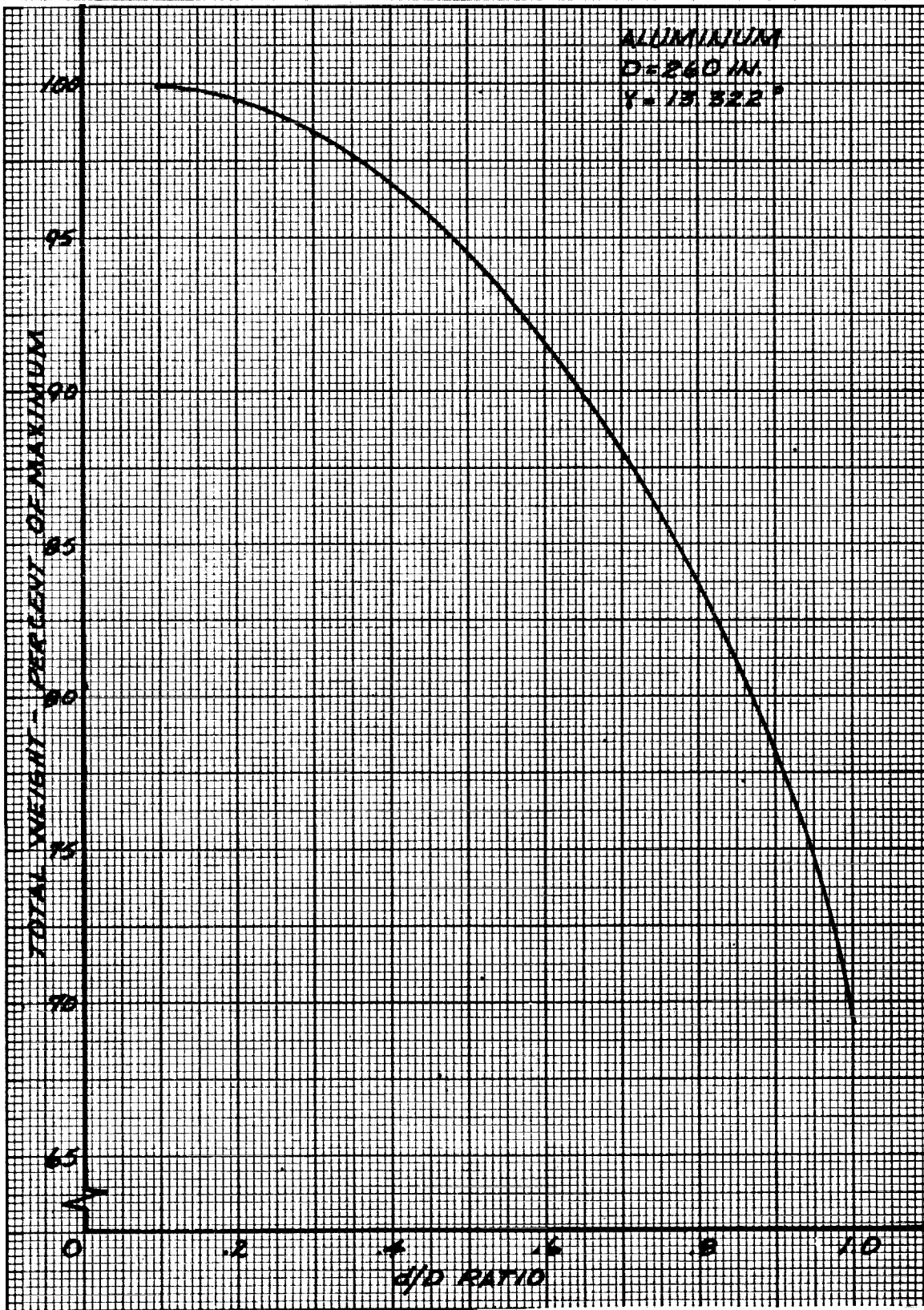


FIGURE 17. PERCENTAGE TOTAL CONE WEIGHT VERSUS  $d/D$  RATIO; BLUNTNESSEFFECT ON TOTAL WEIGHT



## APPENDIX A

## A. PRESSURE DISTRIBUTION

The pressure distribution,  $P_{TOTAL}$ , around the circumference of the cone cross section may be expressed as (Reference 8):

$$P_{TOTAL} = q (C_{p0} + \alpha C_{p\alpha}) + P_{\infty} \quad (A1)$$

where  $q$  = dynamic pressure (psi)

$P_{\infty}$  = ambient pressure,

$C_{p0}$  = zero angle of attack pressure coefficient derived from axial force distribution,

$C_{p\alpha}$  = pressure coefficient, per radian angle of attack, derived from normal force distribution

and  $\alpha$  = angle of attack in radians

From Reference (8), and referring to Figure 1,

$$C_{p0} = \frac{D}{8 a_n} \frac{dC_x}{d(x/D)} \cot \gamma \quad (A2)$$

$$C_{p\alpha} = \frac{D}{4 a_n} \frac{dC_{z\alpha}}{d(x/D)} \cos (180^\circ - \varphi) \quad (A3)$$

Therefore, after substitution in (A1)

$$P_{TOTAL} = \eta q \left[ \frac{D}{8 a_n} \frac{dC_x}{d(x/D)} \cot \gamma + \frac{\alpha D}{4 a_n} \frac{dC_{z\alpha}}{d(x/D)} \cos (180^\circ - \varphi) \right] + P_{\infty} \quad (A4)$$

Since the parameters  $\frac{dC_x}{d(x/D)}$  and  $\frac{dC_{z\alpha}}{d(x/D)}$  (axial and normal force coefficients) have a triangular variation along the longitudinal axis, they may be referred to the maximum ordinate in the following manner:

$$\frac{dC_x}{d(x/D)} = \left[ \frac{dC_x}{d(x/D)} \right]_0 \frac{2L}{D} \tan \gamma, \text{ and} \quad (\text{A5})$$

$$\frac{dC_{z\alpha}}{d(x/D)} = \left[ \frac{dC_{z\alpha}}{d(x/D)} \right]_0 \frac{2L}{D} \tan \gamma. \quad (\text{A6})$$

Therefore, assuming ambient pressure inside the cone,

$$P_o = P_{\text{TOTAL}} - P_\infty$$

substitution of the above relationships into (A4), and setting

$$a_n = L \tan \gamma$$

the net pressure,  $P_o$ , becomes

$$P_o = \eta q \left\{ \frac{1}{4} \left[ \frac{dC_x}{d(x/D)} \right]_0 \cot \gamma + \frac{\alpha}{2} \left[ \frac{dC_{z\alpha}}{d(x/D)} \right]_0 \cos (180^\circ - \varphi) \right\}, \quad (\text{A7})$$

#### B. BENDING MOMENT AND AXIAL FORCE:

The normal force acting upon an incremental cone length  $d(x/D)$  is given as (Figure 18):

$$F(x/D) = (\alpha \text{ rad}) \frac{dC_{z\alpha}}{d(x/D)} d(x/D) q \left( \frac{\pi D^2}{4} \right), \quad (\text{A8})$$

At any distance,  $L/D$ , from the nose of the cone, the normal force is given by

$$F = \frac{\pi q D^2}{4} \int_{X/D}^{X/D - L/D} (\alpha \text{ rad}) \frac{dC_{z\alpha}}{d(x/D)} d(x/D). \quad (\text{A9})$$

Again, referring to the triangular relationship, the following substitutions may be made:

$$\frac{dC_{z\alpha}}{d(x/D)} = \left[ \frac{dC_{z\alpha}}{d(x/D)} \right]_0 \left[ 1 - \frac{2x}{D} \tan \gamma \right], \quad (A10)$$

$$X/D = \frac{1}{2 \tan \gamma}$$

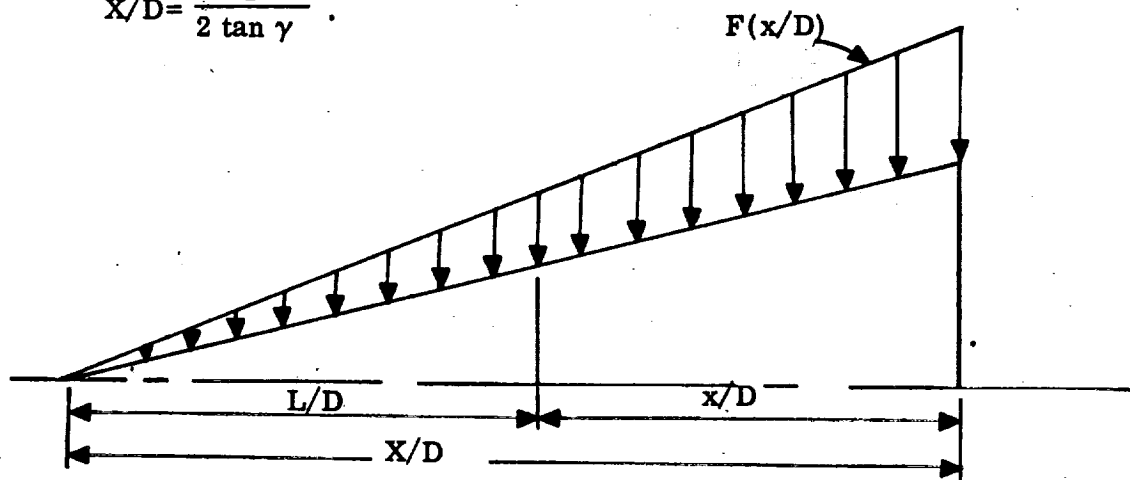


FIGURE 18. NORMAL FORCE LOADING SCHEMATIC

Upon integrating Equation A9, one obtains the following expression:

$$F_B = \frac{\alpha \pi q D^2}{4} \left[ \frac{dC_{z\alpha}}{d(x/D)} \right]_0 \frac{L^2}{D^2} \tan \gamma \quad (A11)$$

The moment arm of this force with respect to the arbitrary station,  $L/D$ , is  $L/3D$ , and the resultant bending moment expression at any station may now be written as

$$M = \frac{\pi \alpha q D^2}{4} \left[ \frac{dC_{z\alpha}}{d(x/D)} \right]_0 \frac{L^3}{3D^3} \tan \gamma. \quad (A12)$$

Similarly, the axial force at any station may be expressed by Equation A13 as:

$$F_A = \frac{\pi q D^2}{4} \left[ \frac{dC_x}{d(x/D)} \right]_0 \frac{L^2}{D^2} \tan \gamma \quad (A13)$$

### C. LOAD PER INCH OF CIRCUMFERENCE:

The axial load per inch,  $N_A$ , is obtained by dividing the axial force Equation A13 by the perimeter at  $L/D$ ,  $2\pi a_n$ :

$$N_A = q \frac{L}{8} \left[ \frac{dC_x}{d(x/D)} \right]_0 \quad (A14)$$

The bending load per inch,  $N_B$ , is obtained from the familiar flexure formula,  $f = \frac{Mc}{I} = \frac{N_B}{t}$ , from which

$$N_B = \frac{\alpha q L}{12 \tan \alpha} \left[ \frac{dC_{z\alpha}}{d(x/D)} \right]_0 \cos \varphi \quad (A15)$$

A positive value from Equations A14 and A15 indicate compression.

In the above Equation A15,  $\cos \varphi$  accounts for the load variation about the periphery and will cause  $N_B$  to be negative over one half of this periphery. In all instances, however, the minimum crushing pressure (hoop compressive stress) occurs at the point of maximum axial compressive stress and vice-versa.

## APPENDIX B

## A. GENERAL AERODYNAMICS

The pressure coefficient,  $C_p$ , and the total normal force coefficient gradient,  $C_{z\alpha}$ , with angle of attack for pointed cones are provided in conical flow tables (Reference 4). The reference provides data only on sharp cones in supersonic flow in which the shock is attached and the flow is conical. For these same conditions, the overall center of pressure is at,

$$\frac{CP}{D} = \frac{2}{3} \frac{X}{D^2} + \frac{\tan \gamma}{3} \quad (B1)$$

and the local normal force coefficient gradient can be expressed in terms of the total normal force as

$$\frac{dC_{z\alpha}}{d(x/D)} = 4 \tan \gamma C_{z\alpha} \frac{L}{X} \quad (B2)$$

using the notations of Figure 18.

For blunted cones or spheres, test data is generally utilized to obtain these values unless the Mach number is high enough for the hypersonic impact theory to apply.

With respect to axial force distributions, if a local pressure distribution,  $C_p$ , is defined at  $\alpha = 0$  degrees, the local axial force can be defined as

$$\frac{dC_x}{d(x/D)} = \frac{8a_n}{D} \tan \gamma C_p \quad (B3)$$

## B. CONE LOADS

In this report, the shape parameters are defined by a series of pointed cones and by a single blunted cone of  $13.322^\circ$  half angle. This unique cone was selected since an abundance of test data was available, both wind tunnel and flight. The enclosed curves provide the external loading conditions for all shapes.

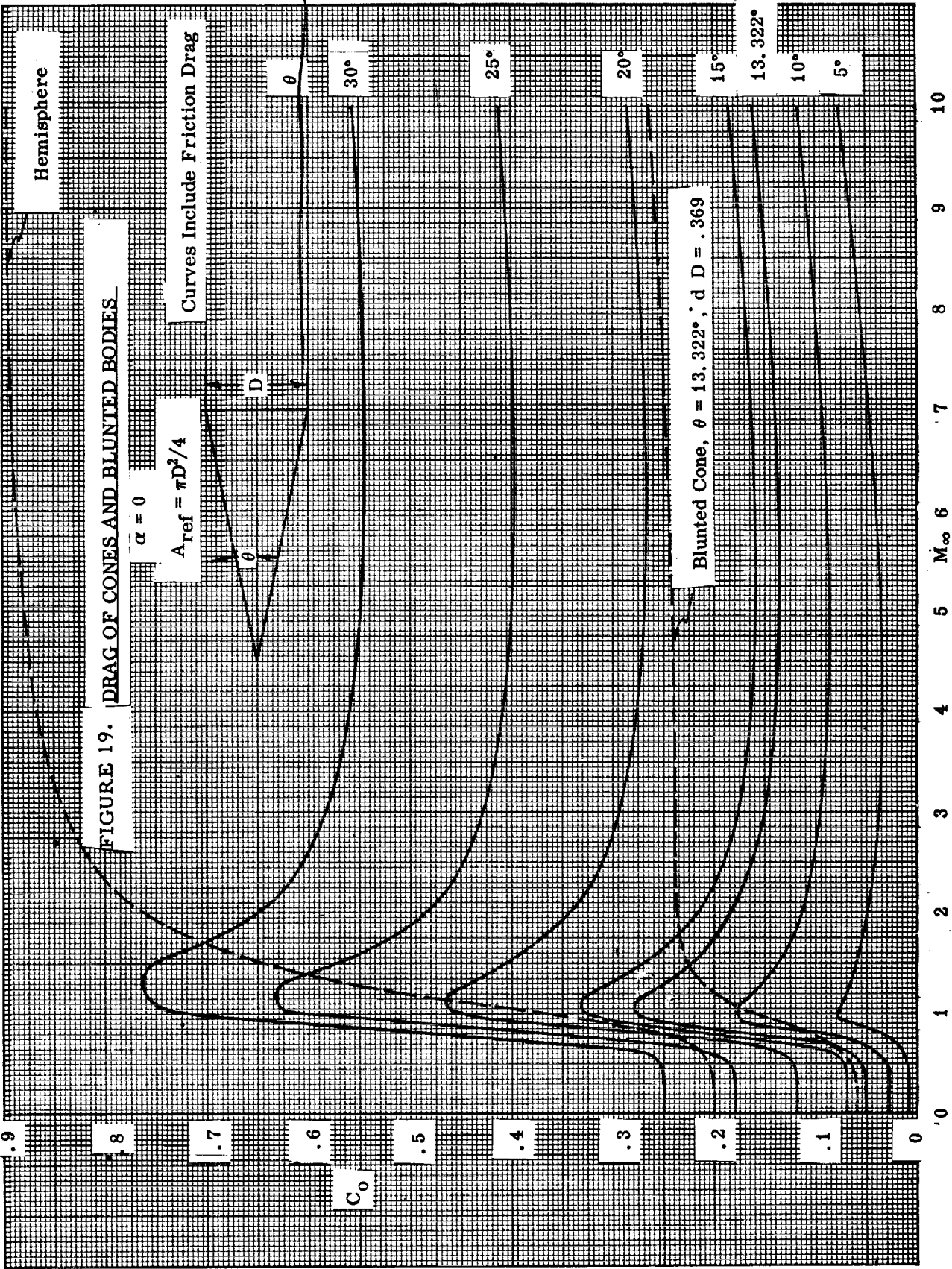


FIGURE 20. LOADS ON NOSE SHAPES

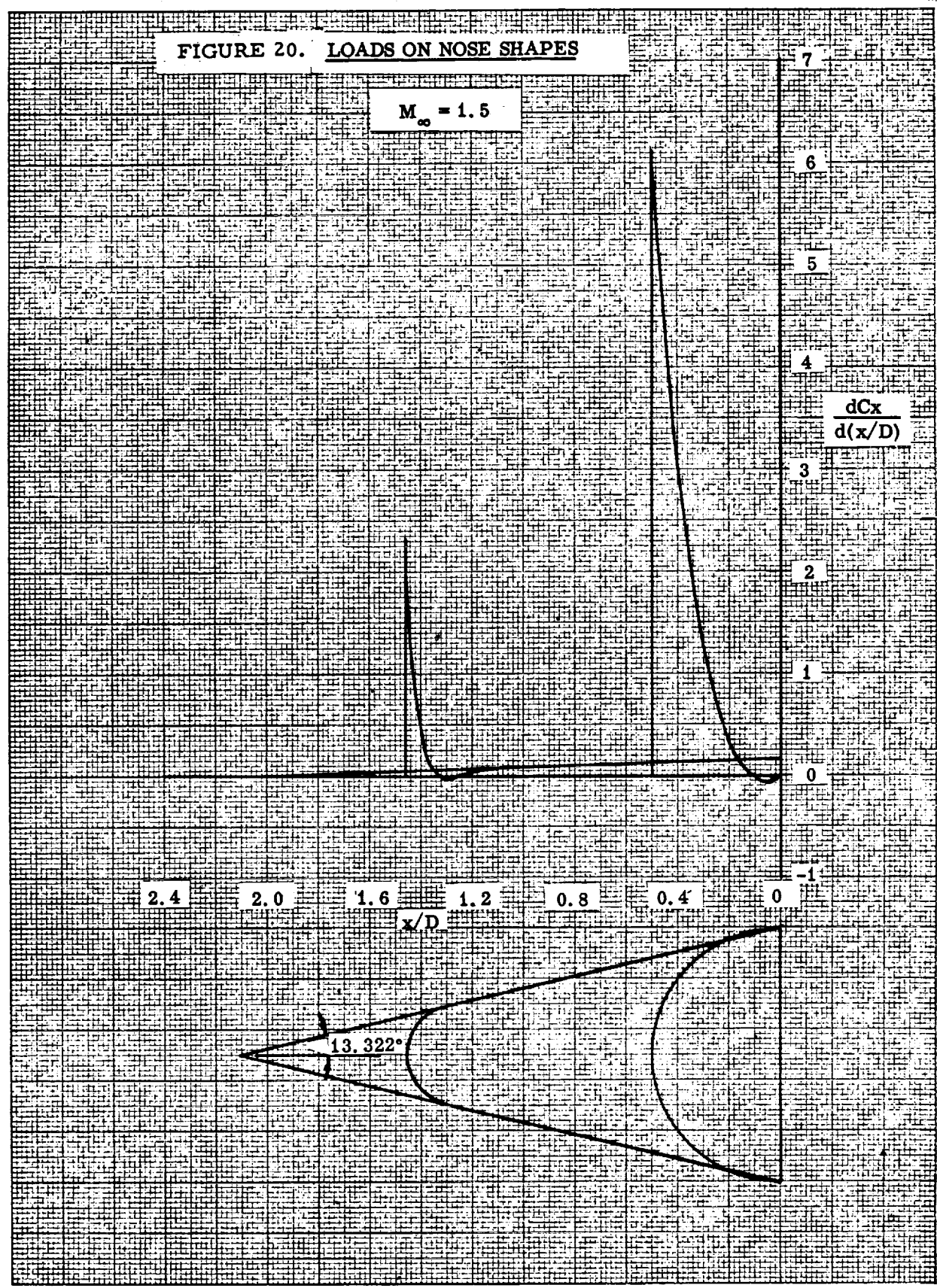


FIGURE 21. LOADS ON NOSE SHAPES

$M_{\infty} = 1.5$

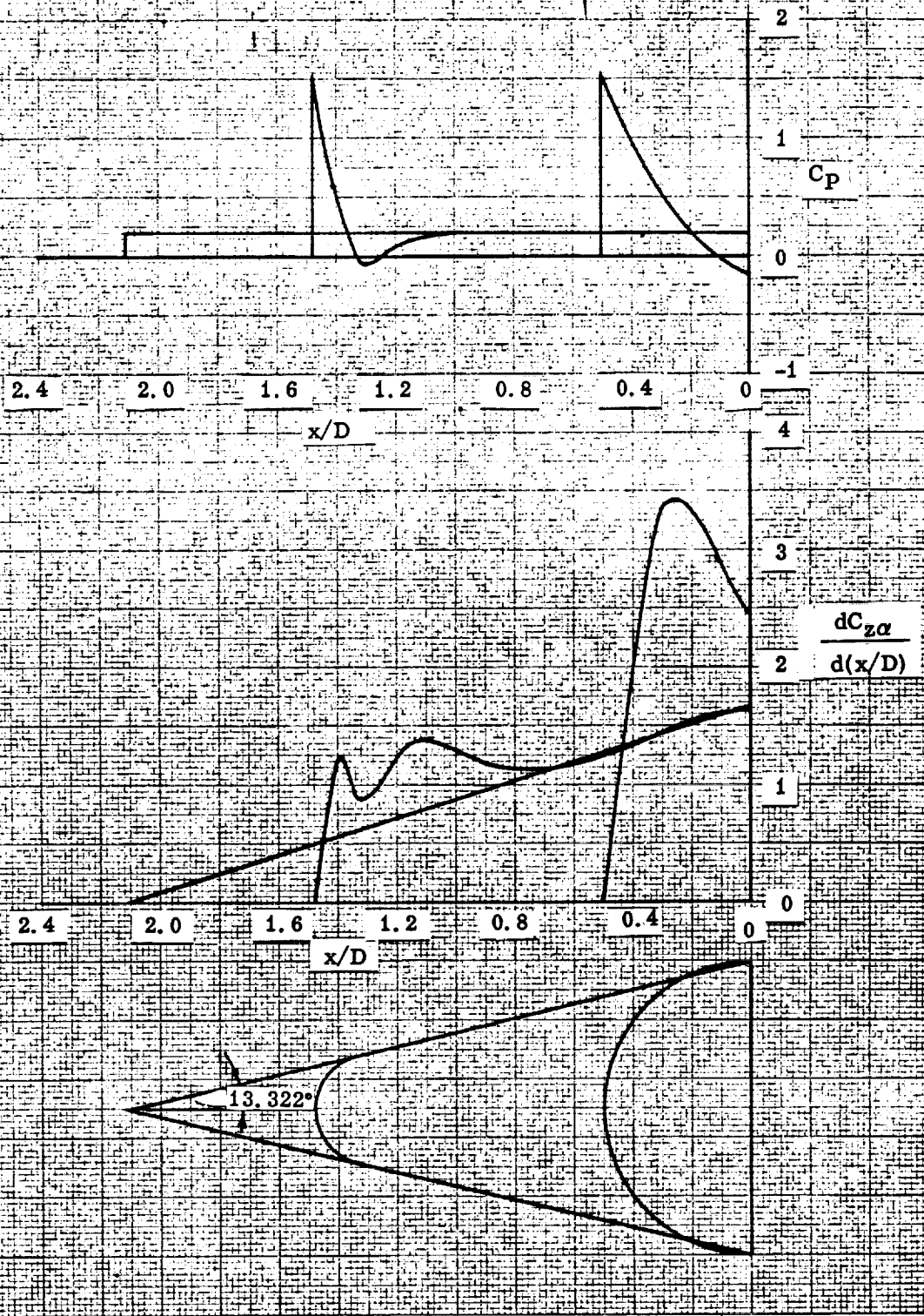
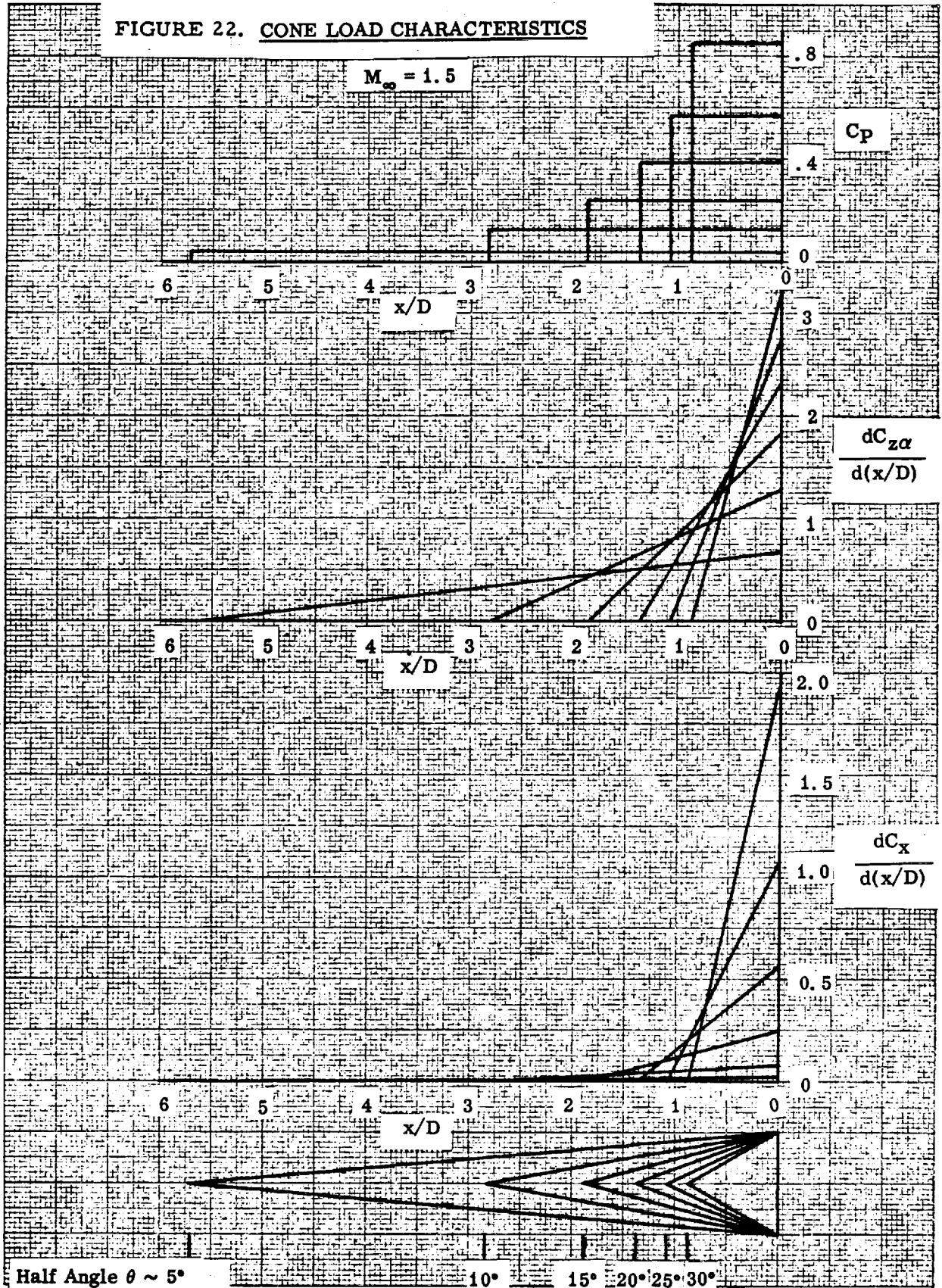




FIGURE 22. CONE LOAD CHARACTERISTICS



## REFERENCES

1. Nickell, E. H. and R. F. Crawford, "Structural Shell Optimization Studies," Lockheed Missiles and Space Co., Sunnyvale, Calif., Report No. 3-42-61-2, Vol. 2, June 1961.
2. Kazimi, M. I., "Sandwich Cylinders," Part II, Aerospace Engineering, Vol. 19, No. 9, 1960, pp 34-45.
3. Norris, C. B., and J. J. Zahn, "Design Curves for the Buckling of Sandwich Cylinders of Finite Length Under Uniform External Lateral Pressure," U. S. Forest Products Laboratory, Report No. 1869, May 1959.
4. Kopal, Zdenek, "Tables of Supersonic Flow Around Yawing Cones," Massachusetts Institute of Technology, Technical Report No. 3, 1947.
5. Mushtari, Kh. M and A. V. Sachenkov, "Stability of Cylindrical and Conical Shells of Circular Cross Sections, with Simultaneous Action of Axial Compression and External Normal Pressure," National Advisory Committee for Aeronautics, Technical Memo. 1433 (Translation), April 1958.
6. Bowie, Oscar L., "Design Criterion for Circumferential Ring Stiffeners for a Cone Loaded by External Pressure," Watertown Arsenal Laboratories, Report No. 893/199, November 1957.
7. Becker, Herbert, "Handbook of Structural Stability," Part VI, National Advisory Committee for Aeronautics, Technical Note 3786, July 1958.
8. Goerner, E., "Circumferential Pressure Distribution over the Skin of a Cone Cylinder or Frustum Configuration with a Given Normal and Axial Force Distribution," Office Memo, January 1956.

APPROVAL

MTP-P&amp;VE-S-63-4

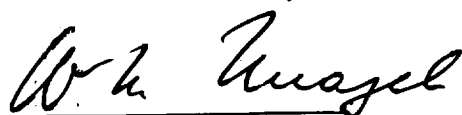
AN INVESTIGATION OF VARIOUS PARAMETERS AFFECTING THE  
STRUCTURAL WEIGHT OF ROCKET VEHICLE NOSE CONES

by

Clyde D. Nevins and Benny W. Helton

The information in this report has been reviewed for security classification. Review of any information concerning Department of Defense or Atomic Energy Commission programs has been made by the MSFC Security Classification Officer. This report, in its entirety, has been determined to be unclassified. This report has also been reviewed and approved for technical accuracy.

  
G. A. KROLL  
Ch, Structures Division

  
WILLIAM A. MRAZEK  
Dir, P&VE Laboratory

## DISTRIBUTION

DIR	M-MS-H
Dr. von Braun	
R-DIR	M-PAT
R-ASTR-DIR	M-HME-P
Dr. Haeussermann	R-P&VE-DIR
R-ASTR-S	Dr. Mrazek
Mr. Digesu	Mr. Hellebrand
R-AERO-DIR	R-P&VE-A
Dr. Geissler	Mr. Goerner
R-AERO-T	R-P&VE-AN
Mr. Reed	Mr. Jordan
R-AERO-A	Mr. Saxton
Mr. Dahm	R-P&VE-AD
Mr. Holderer	Mr. Neighbors
R-AERO-AD	Mr. Laue
Mr. May	Mr. Schwartz
Mr. Few	Mr. Johns
Mr. Linsley (5)	Mr. Wales
Mr. Dunn	Mr. Madewell
Mr. McAnnally	R-P&VE-V
Mr. Bacchus	Mr. Palaoro
R-FP	R-P&VE-VS
Mr. Spears	Mr. Kraus
Mr. Vaccaro	Mr. Edwards
Mr. Page	R-P&VE-PT
MS-IP	Mr. Woods
MS-IPL (8)	Mr. Hurley
	R-P&VE-M
	Dr. Lucas

## DISTRIBUTION (CONT'D)

R-P&amp;VE-MM

Mr. La Iacona

R-P&amp;VE-S

Mr. Kroll

Mr. Sterett

R-P&amp;VE-SS

Mr. Frederick (4)

Mr. Coldwater

R-P&amp;VE-SL

Mr. Showers

R-P&amp;VE-SV

Mr. Farrow

R-P&amp;VE-SE

Mr. Sawyer

R-P&amp;VE-SA

Mr. Blumrich

R-P&amp;VE-SAA (15)

JPL

Mr. Ben Waitman (2)

Mr. Lloyd Blomeyer (2)

Scientific and Technical Information Facility (2)

Attn: NASA Representative (S-AK/RKT)

P. O. Box 5700

Bethesda, Maryland

